Title

Neurotensin neurons in the extended amygdala control dietary choice and energy homeostasis.

Journal

Nature Neuroscience, 25(11)

Authors

Beyaz, Semir

Janowitz, Tobias

Shea, Stephen

et al.

Publication Date

2022-11-01

DOI

10.1038/s41593-022-01178-3

Peer reviewed

HHS Public Access

Author manuscript

Nat Neurosci. Author manuscript; available in PMC 2022 November 23.

Published in final edited form as:

Nat Neurosci. 2022 November ; 25(11): 1470–1480. doi:10.1038/s41593-022-01178-3.

Neurotensin neurons in the extended amygdala control dietary choice and energy homeostasis

Alessandro Furlan[1,*], **Alberto Corona**[1,2,4], **Sara Boyle**[1,2,4], **Radhashree Sharma**[1], **Rachel Rubino**[1], **Jill Habel**[1], **Eva Carlotta Gablenz**[1,3], **Jacqueline Giovanniello**[1,2], **Semir Beyaz**[1], **Tobias Janowitz**[1], **Stephen David Shea**[1], **Bo Li**[1,*]

[1]Cold Spring Harbor Laboratory, Cold Spring Harbor, NY 11724, USA

[2]School of Biological Sciences, Cold Spring Harbor Laboratory, Cold Spring Harbor, NY 11724, USA

[3]Ruprecht-Karls-University Heidelberg, Heidelberg, Germany

[4]These authors contributed equally

Abstract

Obesity is a global pandemic that is causally linked to many life-threatening diseases. Apart from some rare genetic conditions, the biological drivers of overeating and reduced activity are unclear. Here, we show that neurotensin-expressing neurons in the mouse IPAC, a nucleus of the central extended amygdala, encode dietary preference for unhealthy energy-dense foods. Optogenetic activation of IPAC^{Nts} neurons promotes obesogenic behaviors, such as hedonic eating, and modulates food preference. Conversely, acute inhibition of IPAC^{Nts} neurons reduces feeding and decreases hedonic eating. Chronic inactivation of IPAC^{Nts} neurons recapitulates these effects, reduces preference for sweet, non-caloric tastants, and, furthermore, enhances locomotion and energy expenditure. As a result, mice display long-term weight loss, improved metabolic health, and are protected from obesity. Thus, the activity of a single neuronal population bidirectionally regulates energy homeostasis. Our findings could lead to new therapeutic strategies to prevent and treat obesity.

Introduction

The prevalence of obesity is increasing worldwide. Although genetic predisposition certainly plays a role, obesity is mostly a consequence of poor dietary choices, maladaptive eating

*Correspondence: alessandro.furlan@ki.se (A.F.); bli@cshl.edu (B.L.).

Author contribution

A.F. and B.L. conceived and designed the study. A.F. conducted the experiments and analyzed data. A.C. assisted with the photometry experiments with food odors and the data analysis. S. Boyle set up behavioral rigs and generated Matlab code for controlling behavioral devices and analyzing photometry data. R.S. assisted with the smFISH experiments. R.R. and J.H. assisted with operating the metabolic cages. E.C.G. assisted with the GTT and ITT experiments. R.S. and E.C.G. collected tissue samples and performed qPCR experiments. J.G. assisted with the EPM and OF experiments. S. Beyaz provided critical reagents. T.J. supervised the experiments by E.C.G. and assisted with interpreting metabolic data. S.D.S. supervised the experiments by A.C. and assisted with analyzing and interpreting the data. A.F. and B.L. wrote the paper with inputs from all authors.

Competing interests: The authors declare no competing interests.

behavior such as hedonic eating (i.e. eating in the absence of hunger), and lack of physical activity[1].

Palatable foods, especially those rich in sugars and fats, are often preferred to healthier alternatives. A highly palatable food's sight, smell, and taste (i.e. its hedonic properties) can outweigh homeostatic energy balance regulation and the circuits regulating satiety[2,3] and induce feeding in the absence of an actual energy deficit[4]. Although poor dietary choice is a major cause of obesity, our understanding of how food preference is established is far from complete.

Palatability drives maladaptive eating behavior such as hedonic and binge eating, which can lead to rapid weight gain. Some schools of thought propose that homeostatic regulatory systems "defend" a genetically pre-determined body weight set-point[5]. This regulation is, however, unbalanced, as it seems to be permissive to weight gain. Efforts to lose excess weight by introducing caloric restriction and exercise routines are fiercely counterbalanced by metabolic adaptations that tend to restore the pre-intervention body weight[6], making current therapeutic efforts insufficient to stem the tide of obesity.

Despite recognition that energy intake and expenditure are tightly linked components of weight regulation[7], most research has focused on identifying the brain circuits contributing to feeding[8], while those regulating energy expenditure via behavior (e.g. locomotion) and metabolic thermogenesis have received less attention. Identification of the brain networks shaping not only dietary choice, but also controlling these behaviors and physiological adaptations, is crucial to devise new therapeutic approaches.

The interstitial nucleus of the posterior limb of the anterior commissure (IPAC) is a major structure of the extended amygdala[9]. IPAC neurons are activated by innate or learned gustatory stimuli[10,11] and they receive dense projections from the insular cortex, a hedonic hotspot[12]. However, to date, no study has addressed the IPAC's role in energy homeostasis. Here, we uncover a critical role for neurotensin-expressing neurons within the IPAC in establishing dietary choice and orchestrating behaviors that impact metabolic health.

Results

$IPAC^{Nts}$ neurons are specifically activated by palatable food

To verify *Nts* expression in the IPAC, we bred Nts^{Cre};*Ai14* mice, in which *Nts*-expressing (Nts^{+}) neurons express the red fluorescent protein tdTomato[13,14]. The expression pattern of *Cre* recapitulated that of endogenous *Nts* in the IPAC of Nts^{Cre} mice (Supplementary Fig. 1a), thus validating the fidelity of this line. We took advantage of *Ai14* expression, in combination with AGRP immunostaining, to outline the borders of the IPAC; and the *fundus striati* (FS)[15] and to distinguish these areas from the bed nuclei of the stria terminalis (BNST, whose neurons are innervated by hypothalamic $AGRP^{+}$ neurons[16]), and the ventral pallidum (VP). We found that dense Nts^{+} cells form a narrow stripe in the IPAC, which merge with the sparser Nts^{+} cells in the FS and the lateral nuclei of the BNST (Fig. 1a, Supplementary Fig. 1 b,c). No Nts^{+} neurons were observed in the ventral pallidum (VP), though it is rich in axon fibers originating from Nts^{+} neurons (Fig. 1a, Supplementary Fig.

1b,c). Single molecule fluorescent *in situ* hybridization (smFISH) confirmed *Nts* expression in the IPAC complex, and its near absence in nearby striatal and VP territories. Virtually all Nts^{+} neurons in the IPAC were GABAergic (Fig. 1b).

Food-restriction creates a negative energy balance and leads to the activation of homeostatic circuits regulating energy intake to restore the balance[17]. To test whether $IPAC^{Nts}$ or FS^{Nts} neurons are involved in this process, we analyzed the expression of *c-Fos*, a molecular marker that is a proxy for neuronal activation, in food-restricted mice (FR, Fig. 1c), mice re-fed with regular chow (FR+chow, Fig. 1d), or mice re-fed a high-fat diet (FR+HFD, Fig. 1e) (Methods). HFD, but not chow, induced a significant increase in *c-Fos* expression in both IPAC and FS regions (Fig. 1f, i). Interestingly, HFD increased *c-Fos* expression in Nts^{+} neurons of the IPAC but not the FS (Fig. 1g, j; Supplementary Fig. 1d,e), implicating *Nts* as a potential marker to genetically access this brain region and its role in energy homeostasis. Conversely, we found an increased representation of Nts^{+} neurons within $c\text{-}Fos^{+}$ neurons when mice were fed HFD, in IPAC, but not FS (Fig. 1h, k). Of note, mice fed chow or HFD had similar food intake (Fig. 1l). These results suggest that $IPAC^{Nts}$ are activated preferentially by the consumption of palatable food, but not necessarily by an energy deficit or by motor programs underlying food consumption.

$IPAC^{Nts}$ neurons encode food preference

Our understanding of how food preference is established is incomplete. Based on our *c-Fos* data, we reasoned that $IPAC^{Nts}$ neurons could encode food palatability and therefore diet preference. To test this hypothesis, we set out to monitor the *in vivo* activity of these neurons in behaving mice consuming diets with differing palatability. We first labelled these neurons with the genetically encoded calcium indicator GCaMP6f[18] by injecting the IPAC of Nts^{Cre} mice with an adeno-associated virus (AAV) expressing GCaMP6f in a *Cre*-dependent manner, then implanted an optical fiber into the same location (Fig. 2a, Extended Data Fig. 1a). This strategy allowed us to record $IPAC^{Nts}$ neuron activity *in vivo*, in behaving animals.

We started by testing the response of $IPAC^{Nts}$ neurons to chow and HFD in food-restricted conditions. When these diets are presented simultaneously, mice strongly prefer HFD to chow (Extended Data Fig. 1b). For this reason, for our testing, chow and HFD diets were presented to mice on consecutive days, in a randomized order (Methods). In hungry mice, we found that the amplitude of the response of $IPAC^{Nts}$ neurons was higher for HFD than chow (Fig. 2b). In order to test whether $IPAC^{Nts}$ neurons are activated by palatable food when sated, we presented sated mice with HFD. Again, $IPAC^{Nts}$ neurons were strongly activated (Fig. 2c). Importantly, since the feeding bout duration was similar (and uninterrupted) for both diets (i.e. 10 seconds, Fig. 2b,c), we conclude that the difference in this response is not due to motor behaviors or a satiety signal, but rather the palatability of the stimulus. Since the most palatable foods are in general the most preferred and sought after (Extended Data Fig. 1b), we hypothesized a role for $IPAC^{Nts}$ in encoding food preference and direct consummatory behaviors.

To test this, we aimed to deliver two stimuli in the same session, therefore creating the condition for a preference to be established. Since taste is one of the most salient

stimuli regulating food preference and intake, we presented food restricted mice expressing GCamp6f in IPAC^{Nts} neurons with equal volumes of tastants with clearly distinct palatability delivered via two spouts (Methods, Extended Data Fig. 1c,d). We presented a liquid fat diet (Intralipid) that is commonly used as liquid food[19] and is highly palatable. We found that, in line with the mice's behavioral preference (Extended Data Fig. 1e), immediately following ingestion, IPAC^{Nts} neurons were more robustly activated by fat than by water (Fig. 2d) in a concentration-dependent manner (Fig. 2e). Similarly, IPAC^{Nts} neurons of food-restricted mice were more robustly activated by sucrose than water (Fig. 2f) and by sucrose than sucralose (a sweet, thus palatable, but non-caloric sugar analog, Extended Data Fig. 1f). These results further indicate that IPAC^{Nts} neurons respond to palatable stimuli and that their activity is scaled by the palatability of the stimuli. To investigate whether the activity of IPAC^{Nts} neurons encode subtle changes in palatability, we water-restricted mice and tested them with an array of non-caloric tastants (representing sweet, bitter, salt, umami, sour) or water (Fig. 2g-i; Extended Data Fig. 1g,h).

If IPAC^{Nts} neurons encode the palatability of a taste stimulus, then we would expect appetitive tastants (e.g. sucralose, sweet) to evoke a higher response and an aversive tastant (e.g. quinine, a bitter, unpalatable, non-caloric compound) to effectively reduce the amplitude of IPAC^{Nts} firing compared to water. Indeed, the IPAC^{Nts} neurons of water-restricted mice were more robustly activated by sucralose than by water (Fig. 2g), and more by water than by quinine (Fig. 2h). Ingestion of salty (Fig. 2i), umami and sour tastants (Extended Data Fig. 1g,h) did not elicit a significantly different response, compared to water. Analysis of the licking behavior, a proxy for preference [20], showed that mice, irrespective of the inner state (hungry or thirsty) licked the spout delivering the preferred tastants more vigorously (Fig. 2d-i; Extended Data Fig. 1f-h). Analysis of the relationship between the responses of IPAC^{Nts} neurons and the licking behavior showed that in the vast majority of cases (90%) these variables were not correlated (Methods, Supplementary Fig. 2). However, we found a strong correlation between the amplitude of the neural response for the preferred tastant and the behavioral preference for that tastant (Fig. 2j, Methods). Altogether, these results suggest that IPAC^{Nts} neuron activity represents tastant palatability and dietary preference.

In addition to taste, the smell of a food also has a major impact on its palatability[21], which undoubtedly influences feeding choices[22,23]. To examine whether IPAC^{Nts} neurons respond to food-related smells, we measured their *in vivo* responses in head-fixed mice (Fig. 3a) presented with food-related odors from: a palatable high-fat diet (HFD) dissolved in mineral oil (MO), unpalatable butyric acid (BA, typically found in spoiled food and responsible for its rotten smell) in MO, and MO alone as the vehicle control (Methods). Notably, we found that IPAC^{Nts} neurons were strongly activated by HFD, but not BA or MO (Fig. 3b-d). These results suggest that IPAC^{Nts} neurons respond to appetitive but not aversive food-related sensory cues.

To determine whether IPAC^{Nts} neuron activity encodes more subtle dietary preference, we presented mice with two pairs of rewarding HFDs with identical nutritional value: (1) HFD^{CO} (coconut-flavored) and HFD^{OO} (olive oil-flavored) diets and (2) white chocolate (WCh) and dark chocolate (DCh), which are among the popular energy-dense foods causing

obesity in humans. Before testing, mice were presented with each diet pair simultaneously in their home cage to ensure familiarity (Methods). All mice showed a clear preference for either HFD^{CO} or HFD^{OO} (Fig 3e) and for WCh over DCh (data not shown). Once the food preference was established, we head fixed these mice to the olfactometer and presented them with the following odors: (1) HFD^{CO}, HFD^{OO}, chow, and MO (Fig. 3f-h, Extended Data Fig. 2a) and (2) WCh, DCh, chow, and MO (Extended Data Fig. 2b-f). We found that irrespective of the metabolic state of the animal (food-restricted or sated), $IPAC^{Nts}$ neurons showed higher responses to energy dense foods (HFDs, chocolate) than to plain chow (Fig. 3f-h, Extended Data Fig. 2c-f), although their response was larger when mice were food-restricted, suggesting odor-alliesthesia[24] (Fig 3i). Notably, when the pre-test idiosyncratic preferences of individual mice for one of the two HFDs were considered (Fig 3e), $IPAC^{Nts}$ neuron responses were larger for the odor of the favored diet, irrespective of it being CO- or OO- flavored (Fig 3j). These data suggest that the activity of $IPAC^{Nts}$ neurons encodes preference independently of the nutritional value of the stimulus. As sensory perception of palatable diets induces $IPAC^{Nts}$ neuron activation even in the absence of hunger, we hypothesized that activation of $IPAC^{Nts}$ neuron might drive maladaptive eating behaviors (e.g. hedonic feeding).

Activation of $IPAC^{Nts}$ promotes hedonic feeding

To assess whether activation of $IPAC^{Nts}$ neurons could result in overfeeding, we selectively activated these neurons in sated mice with optogenetics. For this purpose, we bilaterally injected the IPAC of Nts^{Cre} mice with an AAV expressing the light-gated cation channel channelrhodopsin (ChR2), or GFP (as a control), in a *Cre*-dependent manner. We implanted optical fibers over the infected areas for light delivery (Fig. 4a, Extended Data Fig. 3a). Following recovery from surgery and viral expression, sated mice received pellets of differing palatability, either on consecutive days or simultaneously (Methods). During each food presentation, pulses of blue light (20 Hz, 7-10 mW, 5 minutes duration) were delivered into the IPAC, preceded and followed by 5 more minutes with no light (Fig. 4b; Methods). We found that photostimulation in the ChR2 – but not GFP – mice generally increased intake for all diets (Extended Data Fig. 3b) and liquids (Fig. 4e,f). The effect was larger for the more palatable HFD and WCh when compared to chow and dark chocolate (DCh) (Fig. 4b,c), respectively, and for liquid solutions of sucrose when compared to water or quinine (Fig. 4e; Extended Data Fig. 3g). Consistently, the number and length of feeding bouts were also increased by the photostimulation (Extended Data Fig. 3d,e). Of note, $IPAC^{Nts}$ activation did not induce any feeding on an inedible eraser, suggesting the effect is food-specific, although it enhanced gnawing (Extended Data Fig. 3c, Methods). We found a correlation between the baseline intake (i.e. the mouse preference for a diet, a function of its palatability) and the activation-induced intake of the different diets and liquids (Fig. 4d,f). Next, we repeated the above experiments with two additional pairs of isocaloric foods: (1) plain chow and chow flavored with quinine (Extended Data Fig. 3f) and (2) HFD^{CO} and HFD^{OO} (Fig. 4 g,h) in sated mice. Mice were habituated to HFD^{CO} and HFD^{OO} diets before the start of the experiment and all mice showed a clear preference for HFD^{CO} (Fig. 4g). We found that in both cases, activation of $IPAC^{Nts}$ neurons increased the intake of the more palatable food to a higher degree than the less palatable counterpart in the pair (Fig. 4 h;. Extended Data Fig. 3f). Next, we sought to investigate whether photostimulation

of IPAC^{Nts} neurons might condition flavor preference. After the baseline preference was established, we performed conditioning (Methods) by pairing the less preferred diet with light delivery. After conditioning, we found that, although in most cases conditioning did not completely reverse the original preference, photostimulation increased the preference for the less preferred diet, (Fig. 4i, j).

Activation of IPAC^{Nts} neurons is positively reinforcing

Activation of IPAC^{Nts} neurons effectively supports self-stimulation (Extended Data Fig. 3h, Methods) and induces place preference in a real-time place preference or aversion (RTPP/A) assay (Fig. 4k; Methods), suggesting that it is intrinsically rewarding. To determine whether IPAC^{Nts} self-stimulation was independent of the homeostatic state of the animal[25], we repeated the self-stimulation experiment in mice in neutral (i.e. sated), positive (i.e. over-fed), and negative (i.e. food-restricted) energy balance (Methods). We found that self-stimulation was independent of the internal state of the animal (Fig. 4l). Notably, we found that activation of IPAC^{Nts} neurons caused a significant reduction in movement in both the RTPP/A assay and in an open field test (Extended Data Fig. 3i, j; Methods).

Altogether, these data indicate that activity of IPAC^{Nts} neurons drives feeding proportionate to the palatability of the food and modulates intake and preference, thereby shaping dietary preferences.

Inhibition of IPAC^{Nts} neurons impairs feeding behavior

We then hypothesized that inhibition of IPAC^{Nts} neurons could have opposite effects on energy intake (i.e. feeding). To investigate this, we selectively and transiently inhibited these neurons in sated mice with chemogenetics. For this purpose, we bilaterally injected the IPAC of *Nts*^{Cre} mice with an AAV expressing the the κ-opioid-derived DREADD (KORD)[26], or mCherry (as a control), in a *Cre*-dependent manner (Methods, Fig. 5a). To test whether acute inhibition of IPAC^{Nts} neurons impairs homeostatic feeding, we food-restricted control and experimental mice overnight. The following day, mice were injected with either SalvinorinB (SalB, a selective KORD DREADD activator[26]) or vehicle DMSO (Methods). Chow was re-introduced to the mice 20 minutes later for testing. We found that SALB – but not DMSO – injections impaired re-feeding in KORD but not mCherry mice (Fig. 5b). Next, we tested whether inhibition of IPAC^{Nts} neurons would impair feeding on a palatable high fat diet (HFD) in mice sated on chow. We found that SALB – but not DMSO – injection impaired feeding on HFD in KORD but not mCherry sated mice (Fig. 5c). Of note, no significant change in drinking behaviour or locomotor activity (Fig. 5d,e) was observed, suggesting a specific role for these neurons in the regulation of feeding behaviour.

Inactivation of IPAC^{Nts} neurons promotes weight loss

The reduction of feeding in KORD mice treated with SALB could have important implications for preventing obesity. However, due to the transient nature of the inhibition, this effect is short-lived (Extended Data Fig. 4a). We hypothesized that a more protracted inhibition of IPAC^{Nts} neurons might reduce feeding on HFD in the long term and thus delay or prevent obesity onset. To test this, we bilaterally injected the IPAC of *Nts*^{Cre} mice with a *Cre*-dependent tetanus toxin light chain virus (TeLC mice)[27] or a control virus (GFP

mice) (Fig. 5f; Supplementary Fig. 5b). We confirmed that, in line with our chemogenetic data, inactivation of IPAC^{Nts} neurons impairs homeostatic feeding (Fig. 5g) but not drinking behavior (Fig. 5h). We then monitored behavior and metabolic parameters of TeLC and control mice in metabolic cages (CLAMS, Columbus, Methods). Although inactivation of IPAC^{Nts} neurons impaired energy intake in re-feeding tests (Fig. 5 b,g), it did not impair food (chow) or water intake of the TeLC mice when these were freely available (Fig. 5i and Extended Data Fig. 4c). However, when we replaced chow with HFD we found that, after 4 days, the TeLC mice ate significantly less HFD than control mice (Fig. 5j). Water intake of TeLC mice was also lower (Extended Data Fig. 4d). Consistently, GFP, but not TeLC mice dramatically increased their caloric intake (EI) (Extended Data Fig. 4f) and likely entered a positive energy balance state (Extended Data Fig. 4g). Indeed, after only 4 days of HFD, the body weight of the GFP mice dramatically increased while that of TeLC mice remained stable (Fig. 5k).

We next sought to identify whether the reduction of food intake was due to a deficit in detecting the hedonic or the nutritional features of food. We show that transient inhibition of IPAC^{Nts} neurons reduced feeding on HFD within 30 minutes from meal initiation (Extended Data Fig. 4b), after gustatory inputs and likely before post-ingestive conditioning takes place. Therefore, this result suggests a role for IPAC^{Nts} neurons in encoding hedonic stimuli. To further probe this, we tested the mice's preference for either sucralose (sweet but non-caloric, therefore not eliciting post-ingestive effects) or sucrose (sweet and also caloric) over plain water (Extended Data Fig. 4e). Notably, the TeLC mice showed impaired ability to form a preference for sucralose, but not for sucrose.

Our loss of function data show that inhibition or inactivation of IPAC^{Nts} neurons reduces overeating of palatable energy dense diets, thereby protecting from obesity onset (Fig. 5k). We sought to investigate whether inactivation of IPAC^{Nts} neurons could regulate body weight and have beneficial effects on metabolic health.

We noticed that the TeLC group lost weight within 10 days post-surgery and subsequently stabilized between d10 and d30 (Fig. 6a; Extended Data Fig. 5a), despite food and water being freely available in the home cage. A reduction in body weight is normally caused by an imbalance between energy intake and expenditure (EE). We found that the EE and locomotion of TeLC mice was higher than controls (Fig. 6b-d).

Anxiety and stress-related states can induce hyperactivity[28]. To determine whether our manipulation induced anxiety-related behaviors, we subjected the TeLC mice and GFP control mice to the elevated-plus maze (EPM) and open-field (OF) tests. We found no difference between the two groups in measures of anxiety behaviors in rodents (Supplementary Fig. 3).

These data show that prolonged inactivation of IPAC^{Nts} neurons enhances locomotion and energy expenditure, effectively leading mice to achieve long-term weight loss.

Inactivation of IPAC^{Nts} neurons promotes metabolic health

We sought to investigate whether increased locomotion induced by inhibition of IPAC^{Nts} neurons could have beneficial effects on mouse metabolism. We found that the TeLC group had markedly higher volume of oxygen inhaled (VO_2), higher carbon dioxide released (VCO_2) and lower respiratory exchange ratio (RER) than controls (Fig. 6e,f; Extended Data Fig. 5b-e), suggesting that in TeLC mice the oxidation rate of lipids was enhanced. These behavioral and metabolic changes protected mice from obesity: after 6 weeks in a diet-induced obesity paradigm (DIO), the GFP mice became obese, but in stark contrast, the TeLC mice remained lean (Fig. 6g,h). We sought to identify potential mechanisms protecting the TeLC mice from developing obesity. In mice that switch to a high fat diet, lipid oxidation is not immediately adjusted to match HFD over-intake, resulting in positive energy balance[29]. Interestingly, the TeLC mice displayed a more rapid adaptation to the diet switch compared to control mice, suggesting a higher lipid oxidation rate (Fig. 6i). Further, we found that even when fed a HFD, these mice displayed markedly elevated energy expenditure, VO_2, VCO_2, and locomotion (Extended Data Fig. 5f-i). Since lipid oxidation is enhanced in mice with access to a running wheel[30], it is likely that the enhanced lipid oxidation rate of the TeLC mice is due to their enhanced movement, which partially explains their resistance to weight gain.

Obesity is often comorbid with life threatening conditions, such as diabetes. We tested whether inhibition of IPAC^{Nts} neurons could improve glucose homeostasis. Indeed, we found that blood glucose levels were significantly lower in the TeLC mice than in GFP mice in a glucose tolerance test and in an insulin sensitivity test (Fig 6j,k; Methods). Thus, inhibition of IPAC^{Nts} neurons preserves glucose homeostasis in mice fed a HFD.

Inactivation of IPAC^{Nts} neurons protected TeLC mice from weight gain in the long-term: at endpoint, the body weight of the TeLC mice was still lower than the GFP mice (8 weeks of HFD; Supplementary Fig. 4a). We found no significant differences in organ weight between TeLC and GFP mice (Supplementary Fig. 4b). However, histological analysis revealed a lower amount of lipid droplets in the brown adipose tissue (BAT) (Fig. 6l) and liver (Fig. 6m) of the TeLC mice compared to controls. Consistently, the TeLC mice had less white adipose tissue (WAT), and brown adipose tissue (BAT) (Fig. 6n). The adipocyte size in iWAT and eWAT was correspondingly decreased in these mice (Fig. 6o, p). Furthermore, iWAT of some TeLC mice contained multilocular lipid droplets (Fig. 6o), suggesting lipid browning. In line with this observation, we found that the expression of *Ucp1* (*Uncoupling protein 1*) was higher in the iWAT of TeLC mice compared to controls (Fig. 6q).

Together, these data show that inactivation of IPAC^{Nts} neurons efficiently protects from obesity and related detrimental health effects associated with an unhealthy diet by promoting metabolic changes favoring energy expenditure.

IPAC^{Nts} neurons form a network regulating energy homeostasis

We next sought to understand how IPAC^{Nts} neurons are connected to known feeding systems by mapping their afferent and efferent connections.

In order to map the monosynaptic inputs to IPAC^{Nts} neurons we injected a *Cre*-dependent monosynaptic retrograde rabies system in the IPAC of *Nts*^{Cre} mice (Fig. 7a,b, Methods). We found that IPAC^{Nts} neurons receive inputs (GFP^{+} cells) from several brain regions whose role in feeding and energy homeostasis has been well documented, such as the BNST, the nucleus accumbens (NAc), the paraventricular nucleus of the thalamus (PVT), the tuberal nucleus (TN), the parasubthalamic nucleus (PSTh), and others (Fig. 7b-d). Interestingly, we found inputs from brain areas involved in the perception of taste, such as the insular cortex (Fig. 7d), and odors, such as the piriform and entorhinal cortices (Fig. 7c, d) which could potentially process food-related sensory information and drive consummatory behaviors.

To determine the downstream targets of Neurotensin neurons in the anterior extended amygdala neurons we injected a GFP fluorescent reporter virus in the IPAC of *Nts*^{Cre} mice (in green in Fig. 7e) and an mCherry AAV in the medial BNST of the same mice (mBNST, in red in Fig. 7e). We found that IPAC neurons project to a vast number of brain regions[15]. However, the projection pattern of its *Nts*$^{+}$ neurons appears to be more restricted and includes the EAC (sometimes referred to as the SLEAc)[15], the lateral hypothalamus (LHA), the substantia nigra pars compacta (SNc), and the retro rubral field (RRF) (Fig. 7f). On the other hand, mBNST^{Nts} neurons have distinct projection targets or, if within the same downstream target area, clearly distinct spatial domains from IPAC^{Nts} neurons. (Fig 7f,g; Extended Data Fig. 6a).

The LHA is a highly heterogenous area, regulating energy intake, energy expenditure, autonomic function, food preference, and many other important physiological functions[31].

We hypothesized that activation of the IPAC^{Nts} → LHA pathway could recapitulate the effects on feeding we observed when activating the IPAC^{Nts} somata. First, we performed monosynaptic retrograde tracing experiments by injecting the LHA with the Cholera Toxin B subunit (CT-B) (Methods) and confirmed that IPAC^{Nts} neurons project to this location (Fig. 7h; Extended Data Fig. 6b). Next, we selectively activated these neurons in sated mice with optogenetics, similarly to what we did for testing optogenetic manipulation of the IPAC^{Nts} somata (7i,j; Extended Data Fig. 6c; Supplementary Fig. 5a; Methods). We found that photostimulation in the ChR2 – but not GFP – mice significantly and preferentially increased energy intake on HFD and WCh but not on chow or DCh (Fig. 7k). In addition, photostimulation produced intense gnawing but not consumption of inedible objects (i.e. eraser, Extended Data Fig. 6d) suggesting the effect is food-specific. Lastly, activation of this pathway is rewarding (Extended Data Fig. 6e).

Altogether, these data unveil the network of IPAC^{Nts} neurons and suggest that they might control energy homeostasis by receiving inputs from feeding-relevant regions encoding taste and odor related sensory stimuli (e.g. piriform cortex) and projecting to the LHA to regulate feeding behavior and energy maintenance.

Discussion

Here, we show a role for IPAC^{Nts} neurons in encoding preference for “unhealthy” foods and regulating dietary choices and energy behaviors. IPAC^{Nts} neurons are activated preferentially

by palatable food and hedonic sensory stimuli (i.e. taste, odor). Their response magnitude increases with hunger and stimulus palatability, and strongly correlates with the mouse's preference for the tastant. Of note, the preference for food encoded by IPAC^{Nts} neurons is dissociable from the nutritional value of the stimulus, suggesting a idiosyncratic and nuanced role in shaping dietary choices. Intriguingly, we show that IPAC^{Nts} neurons are rapidly activated by sensory cues that anticipate food presence (e.g. odors) and thus might act, similarly to Arc^{AGRP} cells, as "feed-forward" neurons to guide food seeking and feeding[32,33] . In line with this, we found that IPAC^{Nts} neurons receive strong input from cortical areas that detect and integrate taste (insular cortex) and smell cues (piriform and entorhinal cortex)[12,34-36].

Activation of IPAC^{Nts} neurons promotes intake of diets and liquids as a function of their palatability. However, we also show that activation of IPAC^{Nts} neurons is sufficient to modulate food palatability even once the initial preference is established. This suggests the activity of IPAC^{Nts} neurons is important both for establishing dietary choices and guiding consumption. These effects are dissociable from the diets nutritional value, suggesting that IPAC^{Nts} neurons encode oro-sensorial, rather than solely nutritional, reward stimuli. Importantly, our *c-Fos*, photometry, and activation data suggest that IPAC^{Nts} neurons do not directly represent the specific motor actions of consumption.

Conversely, acute inhibition of IPAC^{Nts} neurons impairs feeding in hungry mice and reduces feeding on HFD in sated mice, while it does not seem to affect homeostatic drinking or locomotor activity. These findings further suggest a specific role for IPAC^{Nts} neurons in regulating energy homeostasis. Chronic inhibition (i.e. inactivation) of IPAC^{Nts} neurons' activity demonstrates that the acute deficit on feeding observed with transient inhibition can be extended for days, reduce caloric intake, and prevent weight gain.

We propose that the feeding deficit is mainly due to disrupted oro-sensorial perception. Photometry data show that IPAC^{Nts} neurons are rapidly activated when stimuli are presented. Furthermore, feeding deficits in acute inhibition experiments appear before post-ingestive effects are likely to take place (less than 30 minutes). In line with this, we show that inactivation of IPAC^{Nts} neurons impairs the mouse's ability to establish a preference for a tastant solely based on the perception of its hedonic value (i.e. taste), over longer periods (i.e. 72h), whereas TeLC mice's ability to form a preference for caloric compounds (eliciting post-ingestive effects) is intact. These results are consistent with previous findings suggesting that hedonic and homeostatic circuits are only partially overlapping[8]. For example, *Trpm5*-deficient mice are unable to sense sweet taste but are able to detect sucrose on the basis of its caloric content[37,38].

It is well established that a lack of physical activity is a major cause of the current obesity pandemic[1], and adherence to exercise routines is a first-line intervention for treating symptoms of obesity. We show that prolonged inactivation of IPAC^{Nts} neurons causes a dramatic increase in aerobic locomotion and long-term weight loss in non-obese mice. Although it might appear somewhat surprising that acute inhibition of IPAC^{Nts} neurons is not sufficient to elicit changes in energy expenditure, it is not unheard of that transient and chronic manipulation of the same neuronal ensembles can result in clearly different

behavioral output[39]. Along this line, the locomotor effects observed could be mediated by the neuropeptide Neurotensin, whose kinetics are slower[40] than the neurotransmitter GABA. Of note, the Neurotensin Receptor type 1 (*Ntsr1*) was reported to regulate energy expenditure and locomotor behavior in the SNc/VTA complex[41] and we and others showed that Neurotensin-expressing neurons in the IPAC project to this area[42]. Another possibility is that IPAC^{Nts} neurons are heterogeneous, such that some are involved in controlling hedonic eating while others are involved in regulating physical activities. The TeLC inhibition would therefore affect both functions.

TeLC mice were preferentially active during their active phase (i.e. dark cycle) and GFP and TeLC mice had similar locomotion behaviors during anxiogenic tests, suggesting that the increase in physical activity in the TeLC mice is context or state-dependent, and may reflect volitional activities in a familiar environment.

Inactivation of IPAC^{Nts} neurons effectively protects mice from obesity and from the deleterious metabolic consequences of chronic feeding on an unhealthy diet. These adaptations are likely the result of multiple metabolic changes. For instance, TeLC mice adapt more rapidly to a high fat diet than the less active controls and exhibit enhanced lipid oxidation. Further, the fat deposits of TeLC mice dissipate energy by becoming metabolically active[43]. Both adaptations increase energy expenditure and likely contribute to the lean phenotype of the TeLC mice after prolonged exposure to an energy-dense diet. In addition, inactivation of IPAC^{Nts} neurons improves glucose metabolism and reduces lipid accumulation in BAT and liver tissues of the TeLC mice fed the HFD, suggesting a role in preventing BAT dysfunction (i.e., BAT “whitening”)[44] and nonalcoholic fatty liver disease[45] associated with obesity in humans.

Finally, we provide a map of the brain areas upstream and downstream of IPAC^{Nts} neurons. Interestingly, IPAC^{Nts} neurons receive monosynaptic inputs from many brain areas implicated in feeding, energy balance, and in taste and odor perception. In line with previous studies, we found strong local connections within IPAC and with the nearby BNST, to which IPAC is intimately related. Other areas containing satiety regulating neurons and projecting to IPAC^{Nts} neurons include the PVH and the Arc[2,3].

Neurotensin neurons in the anterior part of the extended amygdala (EA) area form a continuum between the IPAC, the FS, and most lateral nuclei of the BNST. We show that IPAC^{Nts} neurons and the *Nts*$^{+}$ neurons in the medial nuclei of the BNST (mBNST^{Nts} neurons) are part of distinct networks. IPAC^{Nts} neurons project to the EAC (sometimes referred to as the SLEAc)[15], the SNc, and the most lateral part of the lateral hypothalamus. Interestingly, activation of the IPAC^{Nts} →LHA pathway induces feeding on energy-dense foods and is rewarding, thus partially recapitulating the behaviors deriving from somata activation. This projection pattern suggests that IPAC^{Nts} neurons might belong to the medial – rather than the lateral – division of the IPAC[15], which was reported to be intimately associated with the BNST and the extended amygdala[15]. Considering the profound degree of interconnection with EA territories, we propose that *Nts*-expressing neurons in the IPAC could label a previously unnoticed more lateral nucleus of the BNST. More experiments are

needed to address whether mBNST^{Nts} neurons projecting to LHA and other regions have similar or distinct roles on feeding and energy homeostasis.

Altogether, our data suggest that the *Nts* gene is a useful marker to genetically access this previously uncharacterized brain area. IPAC^{Nts} neurons appear to be homogeneous in regard to their activity: aversive odors (i.e. butyric acid) do not activate IPAC^{Nts} neurons, suggesting the absence of subpopulations encoding aversive stimuli, as reported by studies investigating the role in learned disgust[10,11] in more posterior IPAC territories. In line with this, IPAC^{Nts} neurons are intrinsically rewarding and their projection pattern is clearly distinct from other *Nts*$^{+}$ populations. Nonetheless, because our investigation has been carried out at the population level, it is possible that a more in-depth characterization of this area might reveal currently unappreciated molecular heterogeneity of its neurons.

In conclusion, we identified a single, extra-hypothalamic population of neurons with crucial roles in promoting metabolic responses via behavior modification. From a therapeutic point of view, these findings are highly relevant as they show that blocking a handful of molecularly-defined neurons 1) leads to long-term weight loss; 2) has beneficial effects on metabolic function; 3) protects from obesity and metabolic syndromes. Conceptually, this brain area is an ideal entry point to unravel the complex brain-metabolism regulatory loop underlying body weight homeostasis.

Methods

1. Animals

Male and female mice of at least 2 months of age were used for all the experiments. Mice were housed in their home cages (2-5 mice per cage), under a 12-h light/dark cycle, with food and water freely available. Ambient temperature (70-72 °F) and humidity (62%) were automatically controlled. All behavioral experiments were performed during the light cycle. All experimental procedures were approved by the Institutional Animal Care and Use Committee of Cold Spring Harbor Laboratory (CSHL) and performed in accordance with the US National Institutes of Health guidelines in an AAALACi accredited facility. The *Nts*^{Cre} mouse line (Stock No: 017525), *Ai14* (Stock No: 007908) and wild-type mice (Stock No:000664) were purchased from Jackson Laboratories and bred onto a C57BL/6J background.

2. Viral vectors

- AAV9-pCAG-Flex-EGFP-WPRE (Addgene #51502)
- AAV5-pAAV-hSyn-DIO-EGFP (Addgene #50457)
- AAV9-EF1a-DIO-hChR2(H134R)-eYFP-WPRE-hGH (Addgene #20298)
- AAV2/9-CAG-DIO-TeLC-eGFP, previously described[27]
- AAV1-Syn.Flex.GCaMP6f.WPRE.SV40 (Addgene, #100833)
- AAV8-pAAV-hSyn-dF-HA-KORD-IRES-mcritrine (Addgene, #65417)
- AAV2-pAAV-hSyn-DIO-mCherry (Addgene, #50459)

- rAAV-nEf1a-DIO-NLS-mCherry-F2A-TVA-RVG.WPRE (Brain VTA, #PT-0027)
- RV-ENVA-ΔG-EGFP (Brain VTA, #R01001)

All viral vectors were aliquoted and stored at −80 °C until use.

3. Stereotaxic surgery

All surgery was performed under aseptic conditions. Mice were placed on a heating pad for the duration of the surgery. Surgical procedures were previously described[46,47]. Briefly, after mice were anesthetized (1–2% isoflurane with oxygen, applied at 1.0 L/minute), they were head-fixed in the stereotaxic injection apparatus. Targeting of brain areas was done using a digital mouse brain atlas (Angle Two Stereotaxic System). Metacam (2mg/Kg) was injected intra-peritoneally as anesthetic.

Once the mouse skull was exposed, we drilled a cranial window (1–2 mm^2), unilaterally (*in vivo* photometry, monosynaptic rabies, anterograde tracing experiments) or bilaterally (opto- and chemo- genetic experiments). Next, a glass pipette was lowered into the window to deliver c.a. 0.1 μL of viral vector to the area of interest (coordinates: IPAC 0.40 mm anterior to Bregma, 1.45 mm lateral from midline, and −4.50 mm vertical from brain surface; BNST: 0.00 mm anterior to Bregma, 0.90 lateral from midline and −4.20 vertical from brain surface). The viral solution was delivered at a rate of ~20 nl/minute, using a Picospritzer III (General Valve) and a pulse generator (Agilent) generating pressure bursts (5–20 psi, 5–20 ms at 1 Hz). Following delivery, the pipette was left in place for 10 minutes, then carefully withdrawn.

For mice for *in vivo* photometry and optogenetics experiments, following viral delivery, we implanted optic fibers above injection locations (coordinates: IPAC: 0.40 mm anterior to Bregma, 1.45 mm lateral from midline, and 4.30 mm vertical from brain surface; LHA: 1.40 mm posterior to Bregma, 1.15 mm lateral from midline, and 5.00 mm vertical from brain surface). When needed, a head-bar was also mounted to facilitate head-restraint. Nts^{Cre} mice used for rabies tracing were first unilaterally injected in the IPAC with the starter AAV. 14 days after, the same mice were injected with the rabies virus. 7 days later, mice were sacrificed, their brain tissue collected and processed for IHC. Nts^{Cre} mice used for anterograde experiments were injected unilaterally in the IPAC and BNST. After 3 weeks mice were sacrificed, their brain tissue collected and processed for IHC. A cohort of wild-type mice were unilaterally injected in the LHA with $Alexa^{555}$-conjugated CT-b (Invitrogen, Thermo Fisher Scientific; 0.2 μl, 1 mg ml−1 in PBS). Mice were perfused 5 days after the injection. Their brain tissue collected and processed for smFISH.

4. *In vivo* fiber photometry experiments in freely moving mice (Fig. 2; Extended Data Fig. 1)

To record the activity of $IPAC^{Nts}$ neurons in behaving animals, we used a commercial fiber photometry system (Neurophotometrics Ltd) and the Bonsai software (v. 2.3.1) to measure GCaMP6f signals through an optical fiber unilaterally implanted above the IPAC (diameter: 200 μm; length: 5.0 mm; NA: 0.37; Inper). Mice were tethered to a patch cord (diameter:

200 μm; Doric Lenses) connected to the photometry system . The intensity of the LED light (λ = 470 nm) for excitation was adjusted to ~20 μW at the tip of the patch cord. Photometry signals and relevant behavioral events were aligned based on an analogue TTL signal and timing data generated by a Bpod State Machine (Sanworks, Stony Brook, NY, USA)[48].

To correct photobleaching of fluorescence signals, we fit a 2-term exponential curve to the data to model photobleaching using Mathworks' fit function. We then used this fitted curve for ΔF/F0 normalization, where ΔF is the change in fluorescence and F0 is baseline fluorescence, treating the fitted curve as baseline fluorescence in our calculation: ΔF/F0 = (F(t) – F0(t)) / F0(t), where F is the raw fluorescence data and F0 is the fitted curve. This gave us a corrected ΔF/F0 that takes into account the slowly decreasing baseline. All photometry trials were randomly interspersed, so the differences seen in liquid responses were not due to bleaching, or to our bleaching correction. The Z-score of ΔF/F0 was then calculated using the mean and standard deviation of the signal during the baseline periods (the pooled 10 second time windows before each stimulus), Z-score(ΔF/F0) = (ΔF/F0 - mean(baseline ΔF/F0))/standard deviation(baseline ΔF/F0).

A small number of trials had artifacts due to coiling of the photometry fibers or movement of the animals. To find these trials, we automatically flagged for review any trial with a fluctuation of greater than 3 times the standard deviation of signal in the control channel. We discarded trials with significant artifacts during the stimulus period. This method minimized the effect of movement artifacts on the signal.

4a. Free-feeding tests (Fig. 2b, c).—Mice were food-restricted starting at 5 p.m. the day before the testing day. Food-restricted mice were presented with either a grain-based pellet (similar to the regular chow; 45 mg/pellet, Bioserv, F0165, 3.43 cal/g) or a lard-based high fat pellet (Envigo custom diet, 4.5 cal/g) on consecutive days. Food presentation was randomized. After food restriction experiments, the same mice were given food and water ad libitum, before being tested in sated conditions, 48-h later, with a lard-based high fat pellet (Envigo custom diet, 4.5 cal/g). All feeding bouts lasted for at least 10 seconds.

4b. Free drinking tests (Fig. 2 d-j; Extended Data Fig. 1).—Mice were water-restricted starting at 5 p.m. the day before the training day. On the training day, the mice learned to acquire water by licking at two adjacent spouts, with each spout delivering equal volumes of water in a random order. The spout also served as part of a custom "lickometer" circuit, which registered a lick event each time a mouse completed the circuit by licking the spout. The training protocol required the mice to lick the spout with a water droplet before moving onto the next trial. A custom software written in MATLAB (Mathworks, R2017a) was used to control the delivery of liquids and record licking events through a Bpod State Machine (Sanworks)[48]. The training consisted of one session of 100 trials. The next day, which was the testing day, the mice were tested with two pairs of liquids (see main text). Each pair of liquids was available in interleaved trials (25 trials each pair, 50 trials in total; inter-trial-intervals, random between 8 and 14-s), and each liquid was delivered from one of the two spouts in equal volume. As the protocol required mice to lick the spouts to progress, we ensured that all of the liquids were consumed. The tubing and spouts were carefully washed between delivering of different liquids. Volume calibration was carried out prior to

every testing. In Fig. 2j, behavioral preference (preference) and the associated Z-score were calculated as follow:

$$Z\ score\ (\%) = \frac{\text{Zscore (AUC)}\ tastant\ A - \text{Zscore (AUC)}\ tastant\ B}{\text{Zscore (AUC)}\ tastant\ A + \text{Zscore (AUC}\ tastant\ B}$$

$$Preference\ (\%) = \frac{\text{Licks / s}\ tastant\ A - \text{Licks / s}\ tastant\ B}{\text{Licks / s}\ tastant\ A + \text{Licks / s}\ tastant\ B}$$

5. *In vivo* fiber photometry experiments in head-fixed mice (Fig. 3; Extended Data Fig. 2)

For photometry experiments with the olfactometer, we used a custom-made fiber photometry system to measure GCaMP6f signals *in vivo*. Green and red emitted fluorescence signals were filtered and split to separate photodetectors and digitally sampled at 6100 Hz via a data acquisition board (National Instruments, Model # NI USB-6211). Peaks were extracted by custom MATLAB software with an effective sampling rate of 211 Hz. Signals from each fiber were corrected for photobleaching by fitting the decay with a double exponential, and then normalized to a Z score. The red signals represent autofluorescence and was used to monitor and correct for potential movement artifacts. The signals in the green channel were transformed back to absolute fluorescence and DF/F was computed. The resulting traces from each recording session were converted to a Z score to compare between subjects. All data analysis was performed using custom written code in MATLAB.

Mice were under head-restraint in front of the output of a custom-built olfactometer. Before the testing, mice were habituated to the setup for 1 hour. The odors were presented using the olfactometer, which contains an eight-way solenoid that controls oxygen flow through eight vials. The vials contained odorants dissolved in mineral oil. The odors presented were: butyric acid (Sigma, Cat. No. #103500; 100 µl dissolved in 5 ml mineral oil), olive oil-based HFD (Envigo; 1 g in 5 ml mineral oil), coconut oil-based HFD (Envigo; 1 g in 5 ml mineral oil), white chocolate (Lindt; 1 g in 5 ml mineral oil), dark chocolate (Ghirardelli; 1 g in 5 ml mineral oil), regular chow (PicoLab Rodent Diet 20, Cat. No. #5053*; 1 g in 5 ml mineral oil), and mineral oil as a control (Sigma, Cat. No. #M3516). Food pellets were crumbled and homogenized to mineral oil for 10 minutes using a vortex mixer. Odorized oxygen was diluted 10:1 into a continuous carrier stream for a total flow of 4 l/minute. To prevent odor accumulation, air was collected behind the animal with a vacuum pump. Odor presentations were 3 s every 30 s while constantly measuring calcium signals in $IPAC^{Nts}$ neurons. Every testing session consisted of 10 trials per odor. Mice in Fig. 3e were familiarized to the coco and olive- based lard diets in 2 consecutive days and preference was tested on the 3rd day and based on their 3h intake (see Food preference tests section). Data in Fig. 3f-j were acquired from mice in Fig. 3e.

6. Behavioral assays

6.1 Optogenetic experiments

6.1.1 Feeding experiments.: Mice sated on regular chow and hydrogel were tethered to the optic-fiber patch cable and habituated to the behavior box for 10 minutes on the day

prior to the testing. On the testing day, following an additional habituation of 5 minutes, a food pellet or a liquid (in a metal cup) was placed on the floor of the box. Feeding behavior was assessed for 5 minutes with laser off (baseline measure), then 5 minutes with light on (20Hz, 7-10 mW measured at the tip of the fiber), and then another 5 minutes with laser off. The food was weighed before and after each of the 5-minute sessions. Foods in Fig. 4b,c, Fig. 7k, Extended Data Fig. 3b,c,f and Extended Data Fig. 6d, were delivered on consecutive days in a randomized order; foods in Fig. 4g,h were presented within the same session (see Food preference tests section). The foods used were: grain-based pellets (similar to the regular chow; 45 mg/pellet, Bioserv, F0165, 3.43 cal/g), sucrose (45 mg/pellet, Bioserv, F0021, 3.83 cal/g), high fat diet (HFD) (Bioserv, S3282, 5.49 cal/g), white chocolate (Lindt, 5.5 cal/g), dark chocolate (Ghirardelli, 5.5 cal/g), HFD^{CO} (Envigo custom diet, 4.5 cal/g), HFD^{OO} (Envigo custom diet, 4.5 cal/g). An eraser from the tip of a pencil was used as inedible object. “Gnawing” was quantified by subtracting the eraser weight after every session from the eraser weight at the beginning of the session. Plain and quinine-flavored grain-based pellets were prepared by immerging the pellets in either water or a 10 mM quinine solution for 10 minutes. Pellets were dried overnight and used for testing the following day.

To score feeding bouts, videos generated from the feeding behavioral assays were analyzed frame by frame using Behavioral Observation Research Interactive Software (BORIS v 7.12.2)[49]. A feeding bout was defined as an event lasting for at least 3 seconds from pellet pickup to either pellet drop or pellet fully consumed.

6.1.2. Drinking experiments.: Liquids presented were: 30% sucrose in water (w/v), 10% sucrose in water (w/v), 0.1% sucralose in water (w/v), 5% fat emulsion (intralipid), NaCl 75mM in water (w/v), 10 mM Citric Acid in water, Quinine 1 mM in water and water. Drinking behavior was assessed for 5 minutes with laser off (baseline measure), then 5 minutes with light on (20 Hz, 7-10 mW measured at the tip of the fiber), and then another 5 minutes with laser off. The liquids were weighed before and after each of the 5-minute sessions. Liquids were presented on consecutive days to sated mice, in a randomized order.

6.1.3. Conditioned flavor preference.: Single housed mice sated on chow were familiarized to the coco and olive- based lard diets in 2 consecutive days. The baseline flavor preference was assessed by presenting mice with the two diets at the same time. Food preference was determined based on their 3h intake, over the second of 2 consecutive test days. Conditioning was carried out for 4 days, with 2 sessions per day. Prior to each session, mice were tethered to the optic-fiber patch cable and habituated to the behavioral chamber for 10 minutes. Conditioning consisted in pairing intracranial light pulses (473 nm, 8-10mW, 30Hz) with the less preferred diet (session 1). 4h later, the same mice were presented with the more preferred diet without photostimulation (session 2). The order of the sessions was inverted every day. Photo stimulation was delivered right after the mouse would spontaneously initiate food intake and lasted for as long as the pellet was consumed (each was 0.5 g). The investigator manually delivered the light pulses. Conditioned flavor preference was tested for 2 consecutive days after conditioning (day 5 and day 6). The preference of these 2 sessions was averaged.

6.2. Chemogenetic experiments—For chemogenetic experiments, experimental KORD and control mCherry mice were given a subcutaneous (s.c.) injection of SalB (10 mg / Kg in DMSO) or control vehicle (DMSO, volume equivalent). After the injection, mice were placed back in their home cage for 20 minutes before starting testing. The order of testing, on different days, was as follow: 1) food restricted mice had access for 1-h to chow; 2) mice sated (on chow) had access for 1-h to lard-based HFD (Envigo); 3) mice sated (on chow) were tested on locomotion assays; 4) water restricted mice had access for 1-h to water. For locomotor assays, mice were first introduced to a new semi-transparent normal sized cage for habituation. The arena was enclosed in a sound-attenuating chamber with a house light on the ceiling. After 30 minutes, mice were injected as described above, re-introduced in the cage and their behavior (total distance travelled) was videotaped for 60 minutes. Data was analyzed using the imaging-processing and tracking software Ethovision XT 5.1 (Noldus Information Technologies).

6.3. Liquid preference tests—To test sated mice's preference between a sucralose solution (0.004%) and water, or between a sucrose solution (1%) and water (Extended Data Fig. 4e), sated mice were singly housed with food and water available *ad libitum* for a week before the start of the experiment. Water was dispensed through a bottle in the cage. After this, a second bottle containing either the sucralose or sucrose solution was added to the cage. Mice were allowed to first habituate to the newly added solution for 24-h, after which their consumption of the solution and water over a 48-h period was measured. The testing of sucralose and sucrose was separated by a 48-h period, during which the mice had access only to water. The positions of the bottles were switched every 24-h to minimize a potential positional effect. Preference was calculated as:

$$Preference\,(\%) = \frac{\text{Intake liquid A} - \text{Intake liquid } B}{\text{Intake liquid} + \text{Intake liquid } B}$$

6.4 Food preference tests—Mice in Fig. 3e and Fig. 4g-j were familiarized with HFD^{CO} and HFD^{OO} for 2 days, during which HFD^{CO} or HFD^{OO} (0.5 g / mouse) was introduced the in the home cage on consecutive days, with chow and water available *ad libitum.* Mice were singly housed. On the test days, both HFD^{CO} and HFD^{OO} diets were presented simultaneously in the home cage and intake was measured at 3-h after the delivery as follow:

$$Preference\ for\ CO\,(\%) = \frac{\text{Intake } HFD^{CO} - \text{Intake } HFD^{OO}}{\text{Intake } HFD^{CO} + \text{Intake } HFD^{OO}}$$

6.5 Real-time place preference test—Mice sated on regular chow and hydrogel were tethered to an optic-fiber patch cable. Mice were introduced to a 23×33×25 cm non-transparent, two-sided Plexiglas chamber and their baseline preference for either side (left or right) was assessed for 10 minutes. Mice were tested across two sessions. In session one, one side was assigned as the photostimulation chamber. Every time the mouse would enter this chamber, 5-ms pulses, 30 Hz, 7-10 mW (measured at the tip of optic fibers) of blue light (473-nm laser (OEM Laser Systems Inc.) were delivered intra-cranially. Photostimulation

ceased when the mouse left the photostimulation side. In the second session, we assigned the other chamber as the photostimulation side, and repeated testing. The behavior of the mice was videotaped with a camera. Ethovision software (Noldus Information Technologies) was used to deliver laser pulses and analyze behavioral parameters.

6.6 Intracranial self-stimulation tests—Mice sated on regular chow and hydrogel were tethered to an optic-fiber patch cable and placed in a non-transparent, custom made behavioral box equipped with two ports, one “active” and one “inactive”. Poking into the “active” port would deliver light into the IPAC or the LHA (5-ms pulses, 20 Hz, 10 mW; λ = 473 nm), whereas poking into the “inactive” port would not. Mice were tested in this setup for up to 1-h.

For testing the impact of nutritional state on self-stimulation behavior, ChR2 mice were trained for two consecutive days, 1-h per day, to nose poke to self-stimulate (delivering light into the IPAC) while sated on regular chow (PicoLab Rodent Diet 20, Cat. No. #5053*). Each nose poke produced a 2-second train of stimulation (5-ms pulses, 20 Hz, 10 mW; λ = 473 nm). Mice were then tested on consecutive days when fed regular chow, a high fat diet for 2-h prior the test (“HFD”, Bioserv, Cat. No. # S3282; Physiological value: 5.49 Kcal/g) or after being food-restricted overnight.

6.7 Open field locomotion test—Open field tests for ChR2 mice were performed in a non-transparent square box of 42×21×15 cm. The arena was enclosed in a sound-attenuating chamber with a house light on the ceiling. Animals were placed in one of the corners of the open field arena at the start of a session. Locomotor behavior was assessed for 10 minutes with laser off (baseline measure), then 10 minutes with light on (30 Hz, 7-10 mW measured at the tip of the fiber), and then another 10 minutes with laser off. Behavior was videotaped and the resulting data analyzed using the imaging-processing and tracking software Ethovision XT 5.1 (Noldus Information Technologies).

6.8 Open field anxiety test—Open field test (OFT) was performed in a nontransparent square box 42.5×42.5×40 cm. This open field arena was enclosed in a sound-attenuating chamber with a house light on the ceiling. At the start of the 10-minutes session, animals were placed in one of the corners of the arena and left free to explore the arena . A light source was held above the open field box and projected intense bright light over a 21x21 cm square zone in the middle of the arena. Behavior was videotaped and the resulting data analyzed using the imaging-processing and tracking software Ethovision XT 5.1 (Noldus Information Technologies).

6.9 Elevated plus maze (EPM) test—The Elevated Plus Maze test is a non-transparent, cross-shaped apparatus made of Plexiglass. It consists of two “closed” arms, enclosed by 15 cm high walls and two “open” arms, without walls. The arms are 30 cm long and 5 cm wide and extended from a central platform (5x5 cm), to allow mice to freely moving across the arms of the setup. The maze was elevated at a height of 55 cm from the ground. At the start of the 10 minutes sessions, mice were placed in the central zone. Behavior was videotaped and the resulting data analyzed using the imaging-processing and tracking software Ethovision XT 5.1 (Noldus Information Technologies).

7. Physiological assays

7.1 Metabolic cages—Mice were singly housed and habituated to the metabolic cages (CLAMS, Columbus) for at least a week before testing, under a 12-h light/dark cycle. Mice used in the control and experimental groups (i.e. GFP and TeLC mice) were age-matched. Locomotor activity (infrared beam breaks in the XYZ axis), energy expenditure (EE), oxygen consumption (VO_2), carbon dioxide production (VCO_2), Respiratory exchange ratio (RER), food intake, and water intake were recorded. Data were exported using the Clax software v2.2.0 and analyzed in Excel (2019). For 72-h visualizations, data were binned in 1-h intervals. White and purple represent light (6:00-18:00) and dark cycles (18:00-6:00), respectively. Heat (re-named energy expenditure, EE), VO_2 and VCO_2 data were normalized to body weight. The mice were first fed with regular chow (PicoLab Rodent Diet 20, Cat. No. #5053*; physiological value, 3.43 kcal/g) and then with HFD (Bioserv, Cat. No. # S3282; physiological value, 5.49 kcal/g). Diets and water were freely available during testing. Gas sensor calibration (CO_2, O_2) of the apparatus was performed before each test. Mouse bodyweight was recorded prior to and after every testing session.

7.2 Insulin tolerance test (ITT) & glucose tolerance test (GTT)—Singly housed mice were transferred to a clean cage, with food removed for 6 hours (9 a.m. – 3 p.m.) before each test. All tests started at 3 pm. For ITT, mice were injected intraperitoneally (i.p.) with 0.5 U/kg body weight insulin (Humulin, Eli Lilly; NDC Code: 0002-8215) in 0.9% sterile saline. For GTT, mice were injected i.p. with 1 g/kg bodyweight glucose (Sigma G5767-25G) in 0.9% sterile saline. There was a 48-h gap between tests, during which food and water were available *ad libitum*. Blood glucose levels were measured in duplicates after injection using the OneTouch Ultra 2 Glucometer (OneTouch).

8. Immunohistochemistry

Immunohistochemistry protocols were previously described[46]. Briefly, mice were deeply anesthetized and perfused with first, 50 ml of PBS, followed by 50 ml of 4% paraformaldehyde (PFA) in PBS. The extracted brains were kept in in 4% PFA overnight (O/N) and the following day were transferred in a 30% sucrose solution (in PBS) at 4 °C. After 48-h, brain tissue was cut on a microtome (Leica SM 2010R). The 50-μm coronal brain sections were incubated with the appropriate primary antibodies, diluted in a PBS solution containing 1% Tween20 (PBS-T, Sigma, Cat. Number: P2287) O/N at 4 °C. The following day the sections were washed in PBS-T, twice, the incubated with the secondary antibody diluted in PBS-T, for 2-h at room temperature. Sections were then washed in PBS-T, twice, incubated with DAPI (4′,6-diamidino-2-phenylindole, Invitrogen, cat. number D1306, 0.5 μg/ml in PBS) for 5 minutes, washed twice again in PBS-T and mounted onto slides with Fluoromount-G (eBioscience, San Diego, California, USA). Images were taken using an LSM 710 or LSM780 confocal microscope (Carl Zeiss, Oberkochen, Germany) and visualized and processed using ImageJ (1.53q) and Adobe Illustrator (CS6, Version 16.0.0).

The primary antibodies used were chicken anti-GFP (Aves Labs, GFP1020, dilution 1:1000), rabbit anti-RFP (1:1,000; Rockland, 600-401-379, 35868), rabbit anti-HA-tag (1:1,000; Cell Signaling, 3724S), rabbit anti-mCherry (1:1,000; Abcam, ab167453, GR3213077-3); goat-anti AGRP (1:200, R&D, AF634). The secondary antibodies

used were: Alexa Fluor 488 donkey anti-chicken (1:1000; Cat. number 703-545-155, Jackson ImmunoResearch); Alexa Fluor 647 donkey anti-chicken (1;1000; Cat. Number 703-606-155, Jackson ImmunoResearch); Alexa Fluor 647 donkey anti-goat IgG (1;1000; Cat. number 703-605-003, Jackson ImmunoResearch); Cy3 donkey rabbit (1:1000; Cat. Number 711-165-152, Jackson ImmunoResearch). DAPI (4',6-diamidino-2-phenylindole, Invitrogen, catalogue number D1306) (0.5 μg/ml in PBS) was used to stain nuclei.

9. Fluorescent *in situ* hybridization

Single molecule fluorescent *in situ* hybridization (ACDBio, RNAscope) was used to detect the expression of *Nts*, *Gad2, Slc17a6 (Vglut2)*, *c-Fos*, and *Cre* in the IPAC and surrounding tissues of adult mice. For tissue preparation, mice were first anesthetized under isoflurane and then decapitated. Brain tissue was rapidly extracted, embedded in M-1 Embedding Matrix (Thermo Scientific, Cat. No. 1310), in cryomolds (Sakura Finetek, Ref 4566) and fresh-frozen on dry ice. Brain tissue was cut on a cryostat (Leica, CM3050 S), to obtain 16-μm sections, collected on slides (VWR Microslides superfrost plus (Cat #48311-703) and stored at −80 °C. Hybridization was carried out using the RNAscope kit (ACDBio). The protocol was previously described[48]. Probes against *Nts* (Cat. No. #420441), *Gad2* (Cat. No. #439371)*, Slc17a6 (Vglut2)* (Cat. No. #319171), *c-Fos* (Cat. No. #316921), and *Cre* (Cat. No. #312281) were applied with a 1:50 dilution to sections. Images were taken using an LSM 710 or LSM780 confocal microscope (Carl Zeiss, Oberkochen, Germany) and visualized and processed using ImageJ (1.53q) and Adobe Illustrator (CS6, Version 16.0.0).

9.1 *c-Fos* experiments.—Mice in the food-restriction (FR) groups had the food was removed at 5 p.m. the day before the testing day. Food was reintroduced to the mice 18-h after food-restriction (between 11 a.m. and 2 p.m.). The foods used were regular chow (PicoLab Rodent Diet 20, Cat. No. #5053*) and lard-based HFD (Bioserv HFD, Cat. No. # S3282). 30 minutes after the food reintroduction, food consumption was recorded, and the mice were sacrificed. The brain tissue was processed for RNAscope. Water (Hydrogel,ClearH20) was available ad libitum until 3-h before the mice were sacrificed Mice and their brain tissues in different groups underwent the experimental procedure in parallel to minimize variability.

10. RNA extraction and qPCR

Approximately 50 mg fat tissue was harvested using sterile instruments, and was frozen in 500 μl Trizol (Thermo Fisher, Cat. No. #15596026) on dry ice and stored at −80 °C until further processing. The tissue was then homogenized by adding a stainless-steel bead (Qiagen, Cat. No. #69989) into each tube and shaking the tubes in the TissueLyser (TissueLyser II, Qiagen, Cat. No. #85300) 2 times for 2 minutes each at 30 Hz. After incubating the homogenate for 5 minutes on ice, 100 μl Chloroform (Sigma-Aldrich, Cat. No. #C2432-1L) was added and the tubes were shaken briefly. After incubating for 3 minutes on ice, the tubes were spun at 12000 g at 4 °C for 15 minutes. Subsequently, the clear top layer was transferred into a fresh tube and 1/10 volume of 3 M sodium acetate (Bioworld, Cat. No. #41920024-4) and Glycogen (Thermo Scientific, Cat. No. #R0551) at a final concentration of 1 μg/ul and 250 μl isopropanol (Fisher Scientific, Cat. No. #S25372) were added. The tubes were inverted to mix the contents and after 10 minutes incubation on

ice, the tubes were spun at 12000 g at 4 °C for 10 minutes. The supernatant was discarded, and the RNA pellet resuspended in 500 µl 75% ethanol. After centrifuging at 7500 g at 4 °C for 5 minutes, the supernatant was discarded, and the RNA pellet left to air dry for 5 minutes and then resuspended in 25 µl RNAse-free water. cDNA was synthesized from 500 ng total RNA using Taqman Reverse Transcription reagents (Thermo Fisher, Cat. No. #N8080234). Quantitative RT-PCR was performed using QuantStudio™ 6 Flex Real-Time PCR System, using Taqman Fast Advanced Master Mix (Thermo Fisher, Cat. No. #4444556) and Taqman Primers. The 2ΔΔCt method was used to quantify relative amounts of product with a housekeeping gene (Gapdh) as endogenous control. Primers used were *Gapdh* (Thermo Fisher, Assay ID: Mm99999915_g1, Cat. No. #4331182) and *Ucp1* (Thermo Fisher, Assay ID: Mm01244861_m1, Cat. No. #4331182).

11. H&E Staining

Tissues were fixed in 4% PFA for 24-h at 4°C, washed in PBS three times at room temperature and dehydrated in 70% ethanol. Subsequently, tissues were embedded in paraffin, cut using a microtome serially to produce 5-µm sections and stained with Hematoxylin and Eosin (H&E). Pictures were taken using a Zeiss Observer microscope equipped with 10x, 20x and 40x lenses.

12. Oil Red O staining

Livers were fixed in 4% PFA for 24 h at 4°C, washed in PBS three times at room temperature and cryopreserved in 30% sucrose in PBS. Tissues were embedded in OCT tissue tek (Sakura, Cat. No. #4583) and 10-µm sections were cut using a Leica Cryostat. Oil Red O staining was performed as previously described[50] including the counterstaining with Hematoxylin (Abcam, Cat. No. # ab220365). Pictures were taken using a Zeiss Observer microscope equipped with 10x, 20x and 40x lenses.

13. Statistical analysis

All statistics are described where used. Statistical analyses were conducted using GraphPad Prism 7 Software (GraphPad). No statistical methods were used to pre-determine sample sizes but our sample sizes are similar to those reported in previous publications[47,48,51]. Data distribution was assumed to be normal but this was not formally tested. All t-tests were two-tailed. Statistical hypothesis testing was conducted at a significance level of 0.05. All mice were randomly assigned to different groups and data collection was randomized whenever possible (see Methods for specific experiments). Data collection and analysis were not performed blind to the conditions of the experiments. Mice that, after histological inspection, had the location of the viral injection (reporter protein) or of the optic fiber(s) outside the area of interest, were excluded.

Extended Data

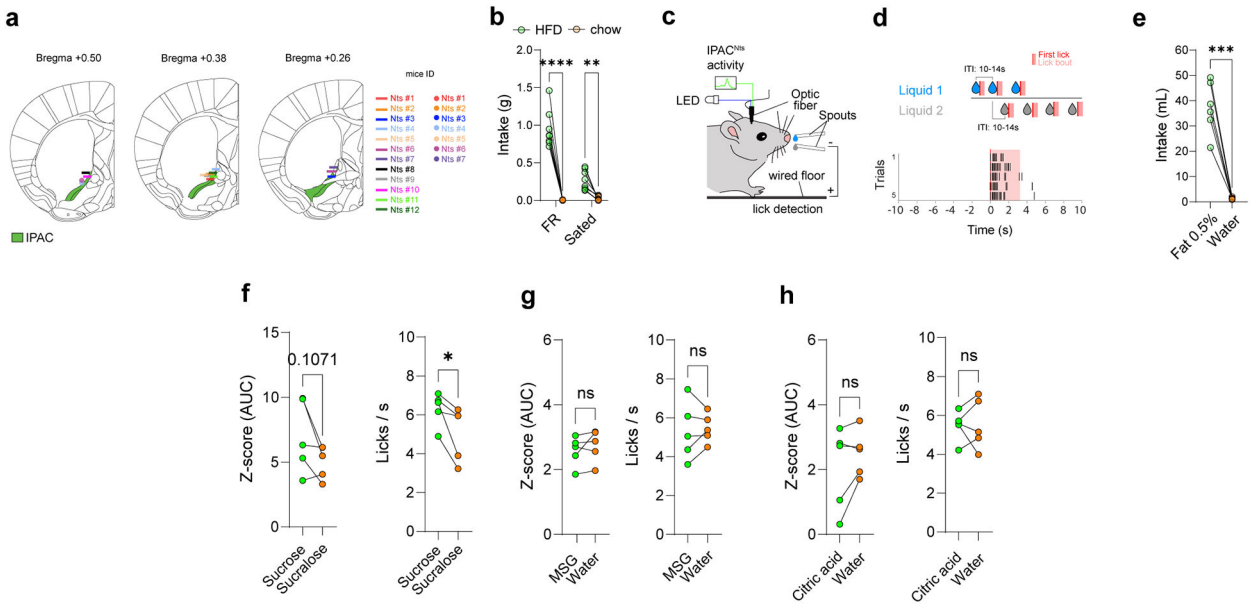

Extended Data Fig. 1. IPAC^{Nts} neurons encode the hedonic value of a stimulus

(a) Schematics showing the locations of optic fiber placement in the mice used in Figure 2 and 3. (b) Feeding behavior of mice when presented with HFD (green) or chow (orange), for 20 minutes, in food restricted (FR, left) or sated condition (right). N=8. Group effect: F(1,7)=95.19, p<0.0001, **p<0.01; ****p<0.0001; Two-way RM ANOVA, Sidak's test. (c, d) Schematics of the experimental setup (c) and task structure (d) used in Figure 2. Bottom panel: representative raster plot showing licking behavior following liquid delivery. (e) Drinking behavior of wild-type mice when presented with Intralipid 0.5% (Fat 0.5%, green) or water (orange), in a 2-bottle preference test, for 72-h, in sated condition. N=6 mice. ***P=0.0003, paired t-test. (f-h) Food-restricted (FR) mice (f) and water-restricted (WR) mice (g, h) were presented with equal volumes of liquids in the same session. Left: Area under the curve (AUC) of GCAMP6f signals. Right: licking behavior (behavior) of mice. AUC and licking behavior were measured in a 3-s window following the first lick. Paired t-tests, n=5 mice/group in all panels. (f) Sucrose (green) or sucralose (orange); AUC: p=0.1071 (n.s.); Behavior: *p=0.0462. (g) Monosodium glutamate (MSG, green) or water (orange); AUC: p=0.3008 (n.s.); Behavior: p=0.7061 (n.s.). (h) Citric acid (green) or water (orange); AUC: p=0.1997 (n.s.); Behavior: p=0.8677 (n.s.).

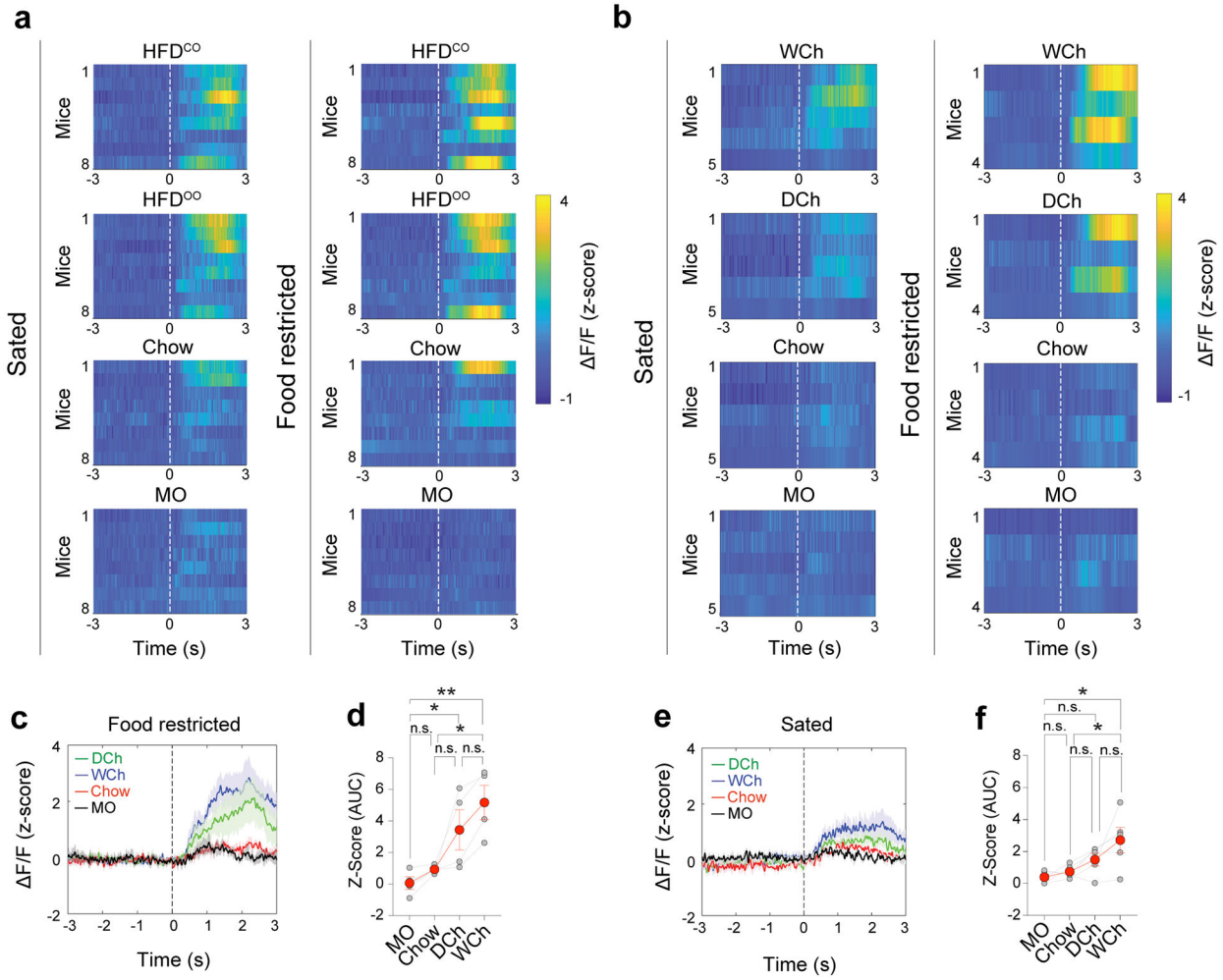

Extended Data Fig. 2. Response of IPAC^{Nts} neurons to odors from several diets

(a, b) Heatmaps of the response of IPAC^{Nts} neurons in individual mice to odors derived from different food sources, under sated or food-restricted condition, as indicated. Dashed lines indicate the onset of odor presentation. (c) Average GCaMP6f signals from IPAC^{Nts} neurons in food-restricted mice aligned to the presentation of different odors (dashed line). (d) Area under the curve (AUC) of the responses in individual mice in (c) in a 3-s window following odor presentation. N=4 mice. $F(3,9)=10.36$, $p=0.0028$; *$p<0.05$, **$p<0.01$, n.s., $p>0.05$; one-way RM ANOVA, Holm-Sidak's test. (e) Average GCaMP6f signals from IPAC^{Nts} neurons in sated mice aligned to odor presentation (dashed line). (f) Area under the curve (AUC) of the responses in individual mice in (e) in a 3-s window following odor presentation. N=5 mice. $F(3,12)=5.169$, $p=0.0160$; *$p<0.05$, $p>0.05$ (n.s); one-way RM ANOVA, Holm-Sidak's test.

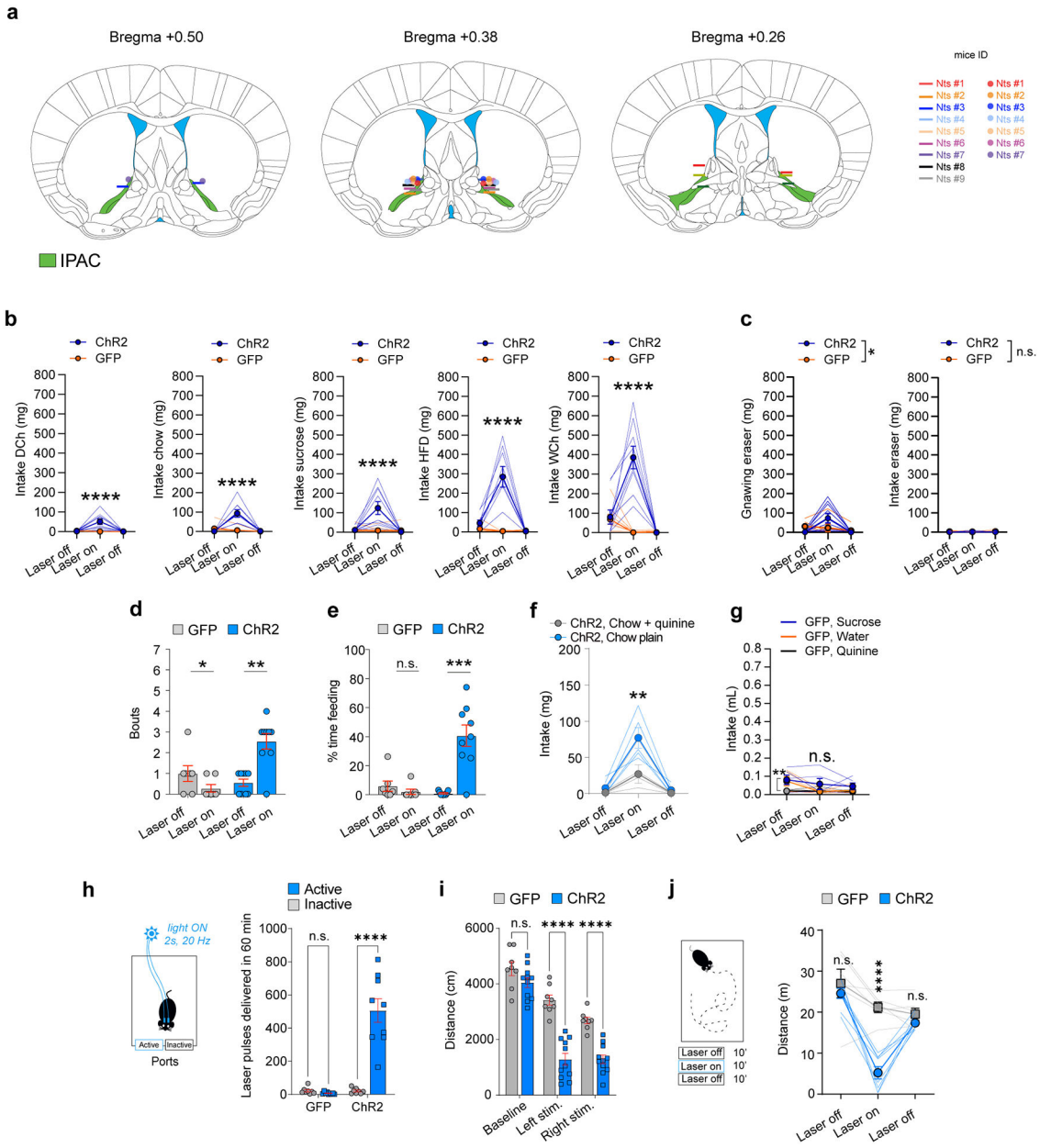

Extended Data Fig. 3. Characterization of behavioral effects following activation of IPAC^{Nts} neurons

(a) Optic fiber placement for mice in Fig. 4. (b) Effect of photostimulation of IPACNts neurons in mice fed dark chocolate (DCh), chow, sucrose, HFD, white chocolate (WCh). ChR2 (n=9) or GFP (n=6) for DCh, ChR2 (n=9) or GFP (n=8) for chow, sucrose, HFD, WCh. Two-way RM ANOVA, Sidak's test. DCh, group effect: F(1,13)=7.374, p= 0.0177; chow, group effect: F(1,15)=8.999, p=0.0090; sucrose, group effect: F(1,15)=7.829, p=0.0135; HFD, group effect: F(1,15)=21.22, p=0.0003; WCh, group effect: F(1,15)=22.56, p=0.0003. (c) Effect of photostimulation of IPAC^{Nts} neurons in mice presented with an inedible pencil eraser. ChR2 (n=9) or GFP (n=6). two-way RM ANOVA, Sidak's test. Gnawing, interaction effect: F(2,26)=4.939, p=0.0152; intake: F(2,26)=1.066, p=3591 (n.s.).

****p<0.0001; p>0.05(n.s.). (d, e) Photostimulation of IPAC^{Nts} neurons increased the number (d) and the duration (e) of feeding bouts in ChR2 (n=9) but not GFP mice (n=7). (d) GFP: *p=0.0465, ChR2: **p=0.0028; (e) GFP: p=0.0982(n.s.), ChR2: ***p=0.0007, paired t-test. (f) Effect of photostimulation of IPAC^{Nts} neurons in ChR2 mice fed quinine-flavored or plain chow pellets (n=5). Interaction effect: F(2,8)=9.476, p=0.0078, **p<0.01, two-way RM ANOVA, Sidak's comparisons test. (g) Effect of photostimulation of IPAC^{Nts} neurons on liquid consumption (control for Figure 4e). GFP mice (n=5), interaction effect: F (4, 16)=1.119, p=0.3820 (n.s.). Two-way RM ANOVA. (h) Self-stimulation paradigm (left) and quantification of the poking responses of ChR2 (n=9) and GFP mice (n=8). Group effect: F(1,15)=37.63, p<0.0001; ****p<0.0001; p>0.05 (n.s.), two-way RM ANOVA, Sidak's test. (i) Distance travelled in the RTPP/A task. ChR2 (n=11) and GFP (n=8) mice. Group effect: F(1,17)=34.11, p<0.0001; ****p<0.0001; p>0.05 (n.s.), two-way RM ANOVA, Sidak's test. (j) Distance traveled in the open field test. ChR2 (n=8) and GFP (n=6) mice. Group effect: F(1,12)=17.30, p=0.0013; ****p<0.0001; p>0.05 (n.s.) two-way RM ANOVA, Sidak's test.

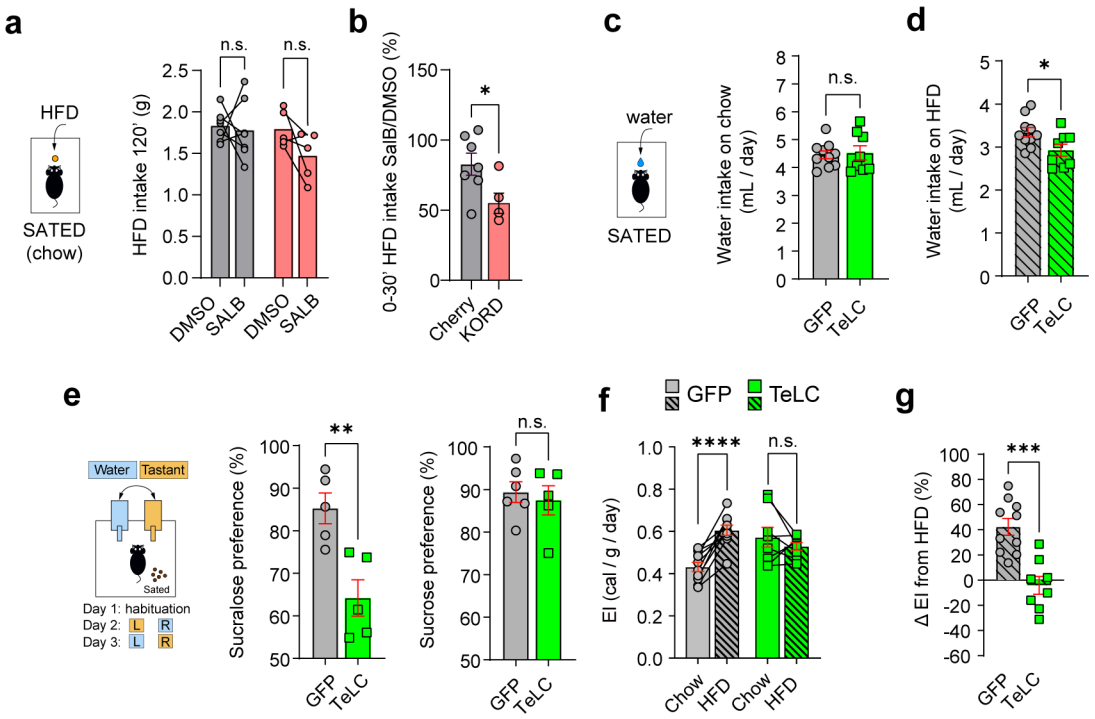

Extended Data Fig. 4. Inactivation of IPAC^{Nts} neurons impairs hedonic perception

(a) HFD intake over a 2-h period in sated NtsCre mice expressing mCherry (gray, control) or KORD (red) injected with DMSO or SalB. mCherry mice, n= 7; KORD mice, n=5. paired t-test. Cherry DMSO-SaLB: p=0.7748, (n.s.); KORD DMSO-SaLB: p=0.1066 (n.s.). Paired t-test.(b) Percentage change of chow intake in food-restricted mice expressing mCherry (gray, control) or KORD (red) when injected with SaLB, normalized to their intake when injected with DMSO, within 30 minutes from food presentation. mCherry mice, n=7; KORD mice, n=5. *p = 0.0326. Unpaired t-test. (c) Daily water intake of the GFP mice (n=10) and TeLC mice (n=8) fed chow. p=0.8023 (n.s.), unpaired t-test. (d) Daily water intake of the GFP mice (n=10) and TeLC mice (n=8) fed HFD. *p=0.0305, unpaired t-test. (e) Schematic

of the 2-bottle preference test (left) for sucralose (center) and sucrose (right). Sucralose: GFP mice (n=5), TeLC mice (n=5): **p=0.0055, unpaired t-test. Sucrose: GFP mice (n=6); TeLC mice (n=5); p=0.6488 (n.s.), unpaired t-test. Legend: L, left bottle, R, right bottle. (f) Comparison of energy intake from chow and HFD diets (derived from Figure 5i and 5j). GFP (n=10): ****p<0.0001; TeLC mice (n=8): p=0.3562 (n.s.); paired t-test. (g) Change in energy intake after the switch from chow to HFD. ***P=0.0002, unpaired t-test.

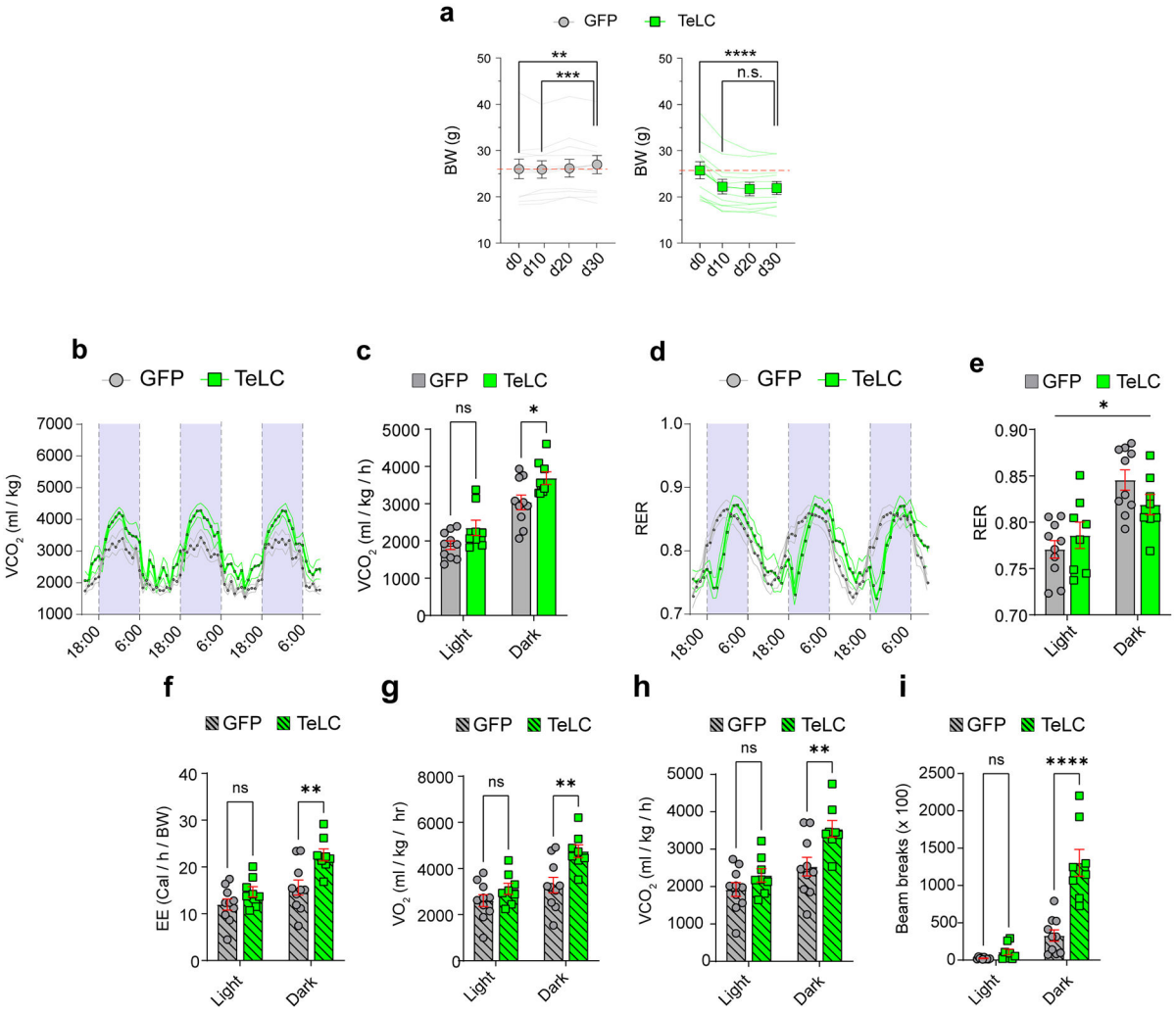

Extended Data Fig. 5. Inactivation of IPAC^{Nts} neurons has positive metabolic effects

(a) Changes in body weight (BW) following injection (d0). GFP mice (n=11): F(3, 30)=6.588, p=0.0015; **p<0.01; ***p<0.001; TeLC mice (n=10): F(3, 27)=28.11, p<0.0001; ****p<0.0001, p>0.05 (n.s.); one-way RM ANOVA, Sidak's test. (b) Volume of carbon dioxide produced (VCO2) by GFP (n=10) and TeLC mice (n=8). Group effect: F(1, 16)=5.745, p=0.0291, two-way RM ANOVA. (c) Average carbon dioxide production (VCO2) of the mice in (b). GFP (n=10); TeLC (n=8). Group effect: F(1, 16)=5.603, p=0.0309; *p<0.05, p>0.05 (n.s.); two-way RM ANOVA, Sidak's test. (d) Respiratory exchange ratio (RER) of GFP (n=10) and TeLC mice (n=8). Interaction effect: F(70,1120) = 5.042, p<0.0001, two-way RM ANOVA. (e) Average RER of GFP (n=10) and TeLC

mice (n=8) fed chow. Interaction effect: F(1, 16)=7.546, *p=0.0143; two-way RM ANOVA, Sidak's test. (f) Average energy expenditure of GFP (n=10) and TeLC mice (n=8) fed HFD. Group effect: F(1, 16)=6.526, p=0.0212; *p<0.05, n.s., p>0.05; two-way RM ANOVA, Sidak's test. (g) Average oxygen consumption (VO2) of GFP (n=10) and TeLC mice (n=8) fed HFD. Group effect: F(1, 16)=6.066, *p=0.0255, p>0.05 (n.s.); two-way RM ANOVA, Sidak's test. (h) Average carbon dioxide production (VCO2) of GFP (n=10) and TeLC mice (n=8) fed HFD. Group effect: F(1, 16)=5.276, *p=0.0355, p>0.05 (n.s.); two-way RM ANOVA, Sidak's test. (i) Average locomotor activity of GFP (n=10) and TeLC mice (n=8) fed HFD. Group effect: F(1,16)=25.21, p<0.0001; ****p<0.0001, p>0.05 (n.s.), two-way RM ANOVA, Sidak's test.

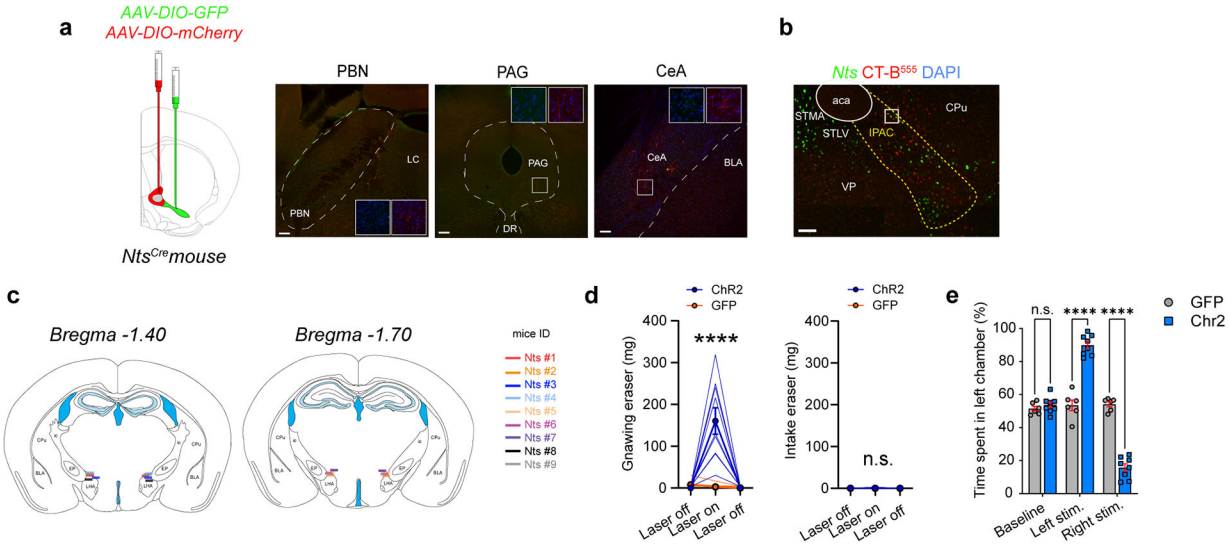

Extended Data Fig. 6. Network of IPAC^{Nts} neurons

(a) Representative images of brain areas innervated by IPAC^{Nts} (green) and mBST^{Nts} (red) neurons. Scale bar: 100 μm. STLV: ventral lateral division of the BNST; STMA: anterior medial division; VP: ventral pallidum; CPu: caudate putamen; IPAC: interstitial nucleus of the posterior limb of the anterior commissure (aca); LC: locus coeruleus; PBN: parabrachial nu.; CeA: central amygdala; BLA: basolateral amygdala; PAG: periacqueductal gray; DR: dorsal raphe. (b) Representative image of smFISH for Nts on retrograde labelled CT-B+ neurons in the IPAC. The square in the image show the high-magnification area showed in Figure 7h (right). Scale bar: 100μm. (c) Schematics showing the locations of optic fiber placement in the mice used in Figure 7. (d) Effect of light delivery into the IPAC of the ChR2 (n=9) or GFP (n=5) mice on gnawing (left) and consumption (right) of inedible items (i.e., pencil eraser). Gnawing (group effect): F(1,12)=11.51, p =0.0053, two-way RM ANOVA, Sidak's test. ****p<0.0001. Intake: (group effect): F(1,12)=0.5327, p=4783, two-way RM ANOVA . (e) Preference of ChR2 (n=8) and GFP mice (n=6) for the left chamber side. Interaction effect: F(2,24)=125.1; p<0.0001; ****p<0.0001; p>0.05 (n.s.). Two-way RM ANOVA, Sidak's test.

Supplementary Material

Refer to Web version on PubMed Central for supplementary material.

Acknowledgments

We thank Taylor Russo for technical assistance, and members of the Li laboratory for helpful discussions. This work was supported by grants from EMBO (ALTF 458-2017, A.F.), Swedish Research Council (2017-00333, A.F.), the Charles H. Revson Senior Fellowship in Biomedical Science (19-23, A.F.), National Institutes of Health (NIH) (R01MH101214, R01MH108924, R01DA050374, R01NS104944, B.L.), the Cold Spring Harbor Laboratory and Northwell Health Affiliation (B.L.), Feil Family Neuroscience Endowment (B.L.), and German Academic Scholarship Foundation (E.C.G.).

Data availability

All data are contained in the main text, extended data or Supplementary Information. Source data are provided with this paper.

Code availability

Custom code is available on Github: https://github.com/Alefurlan/IPACpaper

References

1. Bluher M Obesity: global epidemiology and pathogenesis. Nat Rev Endocrinol 15, 288–298 (2019). [PubMed: 30814686]
2. Fenselau H, et al. A rapidly acting glutamatergic ARC-->PVH satiety circuit postsynaptically regulated by alpha-MSH. Nat Neurosci 20, 42–51 (2017). [PubMed: 27869800]
3. Li MM, et al. The Paraventricular Hypothalamus Regulates Satiety and Prevents Obesity via Two Genetically Distinct Circuits. Neuron 102, 653–667 e656 (2019). [PubMed: 30879785]
4. Zhang X & van den Pol AN Rapid binge-like eating and body weight gain driven by zona incerta GABA neuron activation. Science 356, 853–859 (2017). [PubMed: 28546212]
5. Speakman JR, et al. Set points, settling points and some alternative models: theoretical options to understand how genes and environments combine to regulate body adiposity. Dis Model Mech 4, 733–745 (2011). [PubMed: 22065844]
6. Trexler ET, Smith-Ryan AE & Norton LE Metabolic adaptation to weight loss: implications for the athlete. J Int Soc Sports Nutr 11, 7 (2014). [PubMed: 24571926]
7. Hill JO, Wyatt HR & Peters JC Energy balance and obesity. Circulation 126, 126–132 (2012). [PubMed: 22753534]
8. Rossi MA & Stuber GD Overlapping Brain Circuits for Homeostatic and Hedonic Feeding. Cell Metab 27, 42–56 (2018). [PubMed: 29107504]
9. Alheid GF Extended amygdala and basal forebrain. Ann N Y Acad Sci 985, 185–205 (2003). [PubMed: 12724159]
10. Tanaka DH, Li S, Mukae S & Tanabe T Genetic Access to Gustatory Disgust-Associated Neurons in the Interstitial Nucleus of the Posterior Limb of the Anterior Commissure in Male Mice. Neuroscience 413, 45–63 (2019). [PubMed: 31229633]
11. Tanaka DH, Li S, Mukae S & Tanabe T Genetic recombination in disgust-associated bitter taste-responsive neurons of the central nucleus of amygdala in male mice. Neurosci Lett 742, 135456 (2021). [PubMed: 33290837]
12. Gehrlach DA, et al. A whole-brain connectivity map of mouse insular cortex. Elife 9(2020).
13. Leinninger GM, et al. Leptin action via neurotensin neurons controls orexin, the mesolimbic dopamine system and energy balance. Cell Metab 14, 313–323 (2011). [PubMed: 21907138]

14. Madisen L, et al. A robust and high-throughput Cre reporting and characterization system for the whole mouse brain. Nat Neurosci 13, 133–140 (2010). [PubMed: 20023653]
15. Shammah-Lagnado SJ, Alheid GF & Heimer L Striatal and central extended amygdala parts of the interstitial nucleus of the posterior limb of the anterior commissure: evidence from tract-tracing techniques in the rat. J Comp Neurol 439, 104–126 (2001). [PubMed: 11584811]
16. Steculorum SM, et al. AgRP Neurons Control Systemic Insulin Sensitivity via Myostatin Expression in Brown Adipose Tissue. Cell 165, 125–138 (2016). [PubMed: 27015310]
17. Atasoy D, Betley JN, Su HH & Sternson SM Deconstruction of a neural circuit for hunger. Nature 488, 172–177 (2012). [PubMed: 22801496]
18. Chen TW, et al. Ultrasensitive fluorescent proteins for imaging neuronal activity. Nature 499, 295–300 (2013). [PubMed: 23868258]
19. O'Connor EC, et al. Accumbal D1R Neurons Projecting to Lateral Hypothalamus Authorize Feeding. Neuron 88, 553–564 (2015). [PubMed: 26593092]
20. Tan HE, et al. The gut-brain axis mediates sugar preference. Nature 580, 511–516 (2020). [PubMed: 32322067]
21. Yeomans MR Taste, palatability and the control of appetite. Proc Nutr Soc 57, 609–615 (1998). [PubMed: 10096124]
22. Patel JM, et al. Sensory perception drives food avoidance through excitatory basal forebrain circuits. Elife 8(2019).
23. Riera CE, et al. The Sense of Smell Impacts Metabolic Health and Obesity. Cell Metab 26, 198–211 e195 (2017). [PubMed: 28683287]
24. Cabanac M Physiological role of pleasure. Science 173, 1103–1107 (1971). [PubMed: 5098954]
25. Jennings JH, Rizzi G, Stamatakis AM, Ung RL & Stuber GD The inhibitory circuit architecture of the lateral hypothalamus orchestrates feeding. Science 341, 1517–1521 (2013). [PubMed: 24072922]
26. Vardy E, et al. A New DREADD Facilitates the Multiplexed Chemogenetic Interrogation of Behavior. Neuron 86, 936–946 (2015). [PubMed: 25937170]
27. Murray AJ, et al. Parvalbumin-positive CA1 interneurons are required for spatial working but not for reference memory. Nat Neurosci 14, 297–299 (2011). [PubMed: 21278730]
28. Strekalova T, Spanagel R, Dolgov O & Bartsch D Stress-induced hyperlocomotion as a confounding factor in anxiety and depression models in mice. Behav Pharmacol 16, 171–180 (2005). [PubMed: 15864072]
29. Trajcevski KE, et al. Enhanced lipid oxidation and maintenance of muscle insulin sensitivity despite glucose intolerance in a diet-induced obesity mouse model. PLoS One 8, e71747 (2013). [PubMed: 23951235]
30. O'Neal TJ, Friend DM, Guo J, Hall KD & Kravitz AV Increases in Physical Activity Result in Diminishing Increments in Daily Energy Expenditure in Mice. Curr Biol 27, 423–430 (2017). [PubMed: 28111149]
31. Berthoud HR & Munzberg H The lateral hypothalamus as integrator of metabolic and environmental needs: from electrical self-stimulation to opto-genetics. Physiol Behav 104, 29–39 (2011). [PubMed: 21549732]
32. Chen Y, Lin YC, Kuo TW & Knight ZA Sensory detection of food rapidly modulates arcuate feeding circuits. Cell 160, 829–841 (2015). [PubMed: 25703096]
33. Lowell BB New Neuroscience of Homeostasis and Drives for Food, Water, and Salt. N Engl J Med 380, 459–471 (2019). [PubMed: 30699320]
34. Terral G, et al. CB1 Receptors in the Anterior Piriform Cortex Control Odor Preference Memory. Curr Biol 29, 2455–2464 e2455 (2019). [PubMed: 31327715]
35. Xu W & Wilson DA Odor-evoked activity in the mouse lateral entorhinal cortex. Neuroscience 223, 12–20 (2012). [PubMed: 22871522]
36. Bitzenhofer SH, Westeinde EA, Zhang HB & Isaacson JS Rapid odor processing by layer 2 subcircuits in lateral entorhinal cortex. Elife 11(2022).
37. de Araujo IE, et al. Food reward in the absence of taste receptor signaling. Neuron 57, 930–941 (2008). [PubMed: 18367093]

38. Beeler JA, et al. Taste uncoupled from nutrition fails to sustain the reinforcing properties of food. Eur J Neurosci 36, 2533–2546 (2012). [PubMed: 22712685]
39. Urban DJ, et al. Elucidation of The Behavioral Program and Neuronal Network Encoded by Dorsal Raphe Serotonergic Neurons. Neuropsychopharmacology 41, 1404–1415 (2016). [PubMed: 26383016]
40. Blaha CD & Phillips AG Pharmacological evidence for common mechanisms underlying the effects of neurotensin and neuroleptics on in vivo dopamine efflux in the rat nucleus accumbens. Neuroscience 49, 867–877 (1992). [PubMed: 1436486]
41. Woodworth HL, et al. Neurotensin Receptor-1 Identifies a Subset of Ventral Tegmental Dopamine Neurons that Coordinates Energy Balance. Cell Rep 20, 1881–1892 (2017). [PubMed: 28834751]
42. Woodworth HL, Brown JA, Batchelor HM, Bugescu R & Leinninger GM Determination of neurotensin projections to the ventral tegmental area in mice. Neuropeptides 68, 57–74 (2018). [PubMed: 29478718]
43. Aldiss P, et al. Exercise-induced 'browning' of adipose tissues. Metabolism 81, 63–70 (2018). [PubMed: 29155135]
44. Shimizu I, et al. Vascular rarefaction mediates whitening of brown fat in obesity. J Clin Invest 124, 2099–2112 (2014). [PubMed: 24713652]
45. Recena Aydos L, et al. Nonalcoholic Fatty Liver Disease Induced by High-Fat Diet in C57bl/6 Models. Nutrients 11(2019).

Methods-only References

46. Stephenson-Jones M, et al. A basal ganglia circuit for evaluating action outcomes. Nature 539, 289–293 (2016). [PubMed: 27652894]
47. Zhang X & Li B Population coding of valence in the basolateral amygdala. Nat Commun 9, 5195 (2018). [PubMed: 30518754]
48. Xiao X, et al. A Genetically Defined Compartmentalized Striatal Direct Pathway for Negative Reinforcement. Cell 183, 211–227 e220 (2020). [PubMed: 32937106]
49. Gamba OFM BORIS: a free, versatile open-source event-logging software for video/audio coding and live observations. Methods in Ecology and Evolution 7, 1325–1330 (2016).
50. Mehlem A, Hagberg CE, Muhl L, Eriksson U & Falkevall A Imaging of neutral lipids by oil red O for analyzing the metabolic status in health and disease. Nat Protoc 8, 1149–1154 (2013). [PubMed: 23702831]
51. Stephenson-Jones M, et al. Opposing Contributions of GABAergic and Glutamatergic Ventral Pallidal Neurons to Motivational Behaviors. Neuron 105, 921–933 e925 (2020). [PubMed: 31948733]

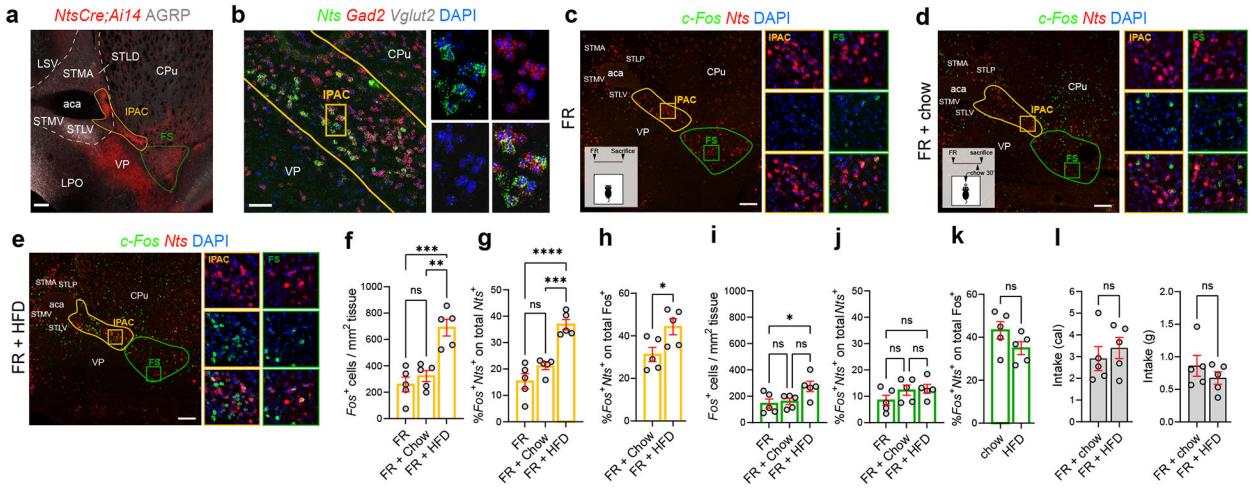

Figure 1. IPAC^{Nts} neurons are activated by palatable food *in vivo*

(a) A coronal brain section containing the IPAC (yellow) and the FS (green) from a representative *Nts^{Cre};Ai14* mouse. Scale bar: 200 μm. STLV/D: ventral/dorsal lateral division of the BNST; STMA/V: anterior medial/ventral division; VP: ventral pallidum; CPu: caudate putamen; LSV: lateral septum; FS: fundus strati; LPO: lateral preoptic area; IPAC: interstitial nucleus of the posterior limb of the anterior commissure (aca). **(b)** A Representative image of IPAC tissue stained for *Nts*, *Gad2* and *Vglut2*. DAPI labels nuclei. Scale bar: 50 μm. **(c-e)** Representative images of IPAC tissue stained for *c-Fos* and *Nts* from food-restricted mice (FR, c), FR mice fed chow (FR + chow, d) and FR mice fed HFD (FR + HFD, e). DAPI labels nuclei. Scale bar: 200 μm. **(f-k)** Quantification of (c-e) in IPAC (f-h, yellow) and FS (i-k, green). N=5 mice in each group; (f): $F_{(2,12)}$=18.16, p=0.0002; (g): $F_{(2,12)}$=26.61, p<0.0001; (h): p=0.0318; (i): $F_{(2,12)}$=4.619, p=0.0325; (j): $F_{(2,12)}$=1.660, p=0.2309; (k): p=0.1393. (f, g, i, j): One-way ANOVA followed by Sidak's multiple comparisons test. ****p<0.0001; ***p<0.001, ***p<0.01; *p<0.05; p>0.05 (n.s.). (h, k): unpaired t-test. **(l)** Quantification of energy intake (calories, left) and food intake (grams, right) and in mice fed chow and HFD. Left: p=0.5295 (n.s.); right: p=0.3450 (n.s.), unpaired t-test.

Data are presented as mean ± s.e.m.

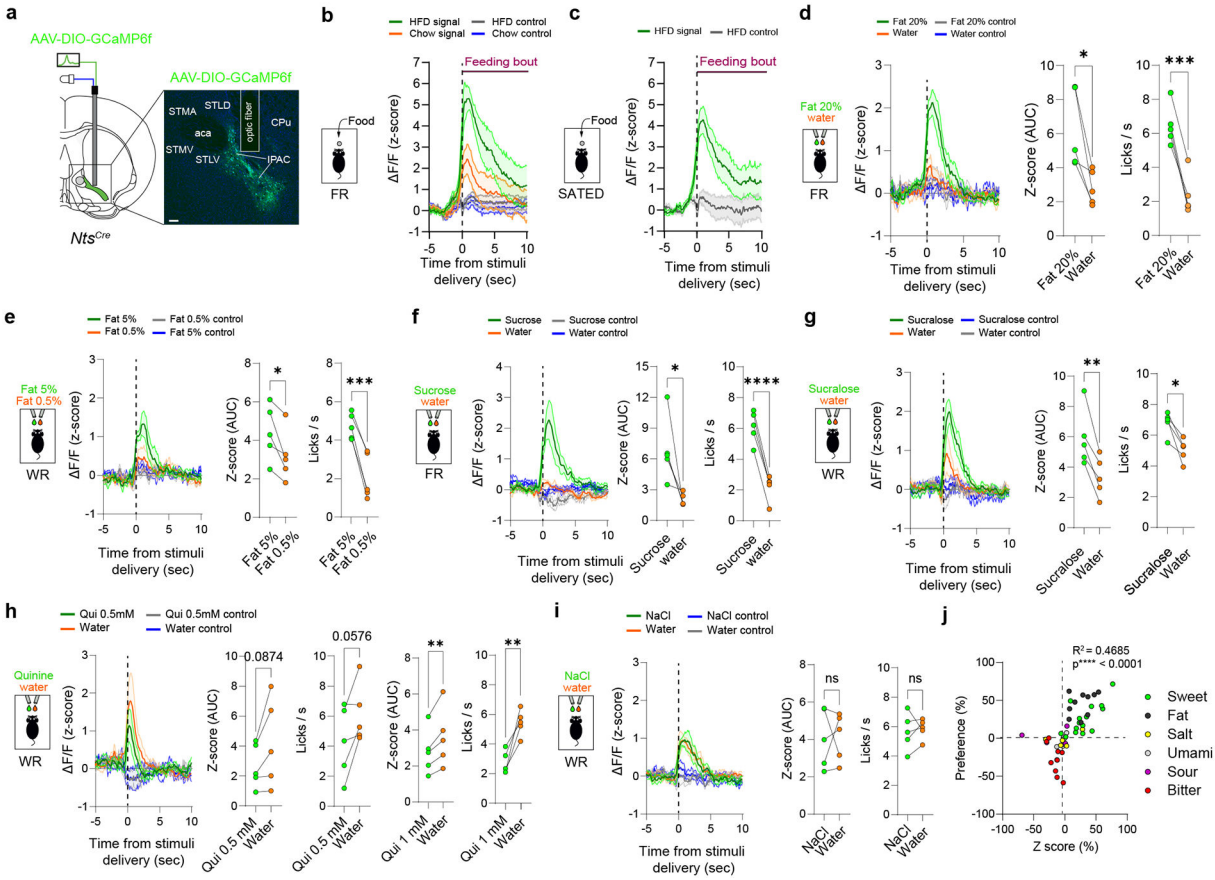

Figure 2. IPAC^{Nts} neurons encode the hedonic value of a tastant

(a) Representative histological image. Scale bar: 100 μm. STLV/D: ventral/dorsal lateral division of the BNST; STMA/V: anterior medial/ventral division; CPu: caudate putamen; IPAC: interstitial nucleus of the posterior limb of the anterior commissure (aca). **(b)** Food-restricted (FR) mice presented with HFD (green trace) or chow (orange trace). Feeding bouts: 10 seconds. Dashed line: stimulus presentation. Gray/blue traces: isosbestic controls. n=5 mice. **(c)** Mice sated on chow presented with HFD. Feeding bouts: 10 seconds. Dashed line: stimulus presentation. Gray trace: isosbestic control. n=7 mice. **(d-i)** Food-restricted (FR) mice (d-f) and water restricted (WR) mice (g-i) were given equal volumes of liquids in the same session. Left: average GCaMP6f signals from IPAC^{Nts} neurons. Dashed line: stimulus presentation (first lick). Center: Area under the curve (AUC) of GCAMP6f signals. Right: licking behavior (behavior) of mice. AUC and licking behavior were measured in a 3-s window following the first lick. Gray/blue traces: isosbestic controls. Paired t-tests, n=5 mice/group in all panels. **(d)** Intralipid (Fat 20%, green trace) or water (orange trace); AUC: *p=0.0234; Behavior: ***p=0.0002. **(e)** Intralipid 5% (Fat 5%, green trace) or Intralipid 0.5% (Fat 0.5%, orange trace); AUC: *p=0.0309; Behavior: ***p=0.0008. **(f)** Sucrose (green trace) or water (orange trace); AUC: *p=0.0388; Behavior: ****p<0.0001. **(g)** Sucralose (green trace) or water (orange trace); AUC: **p=0.0049; Behavior: *p=0.0109. **(h)** Quinine (green trace) or water (orange trace); AUC quinine 0.5 mM – water: p=0.0874; AUC quinine 1 mM – water: **p=0.0095; Behavior quinine 0.5 mM – water: p=0.0576; Behavior quinine 1 mM – water: **p=0.0057. **(i)** Sodium Chloride (NaCl, green trace) or water (orange trace);

AUC: p=0.9292 (n.s.); Behavior: p=0.7136 (n.s.). **(j)** Correlation between the amplitude of GCaMP6f signals from $IPAC^{Nts}$ neurons for a tastant (Z-Score %, x-axis) and licking behavioral preference for such tastant. ****P<0.0001, R^2=0.4685. Pearson correlation test. Data are presented as mean ± s.e.m.

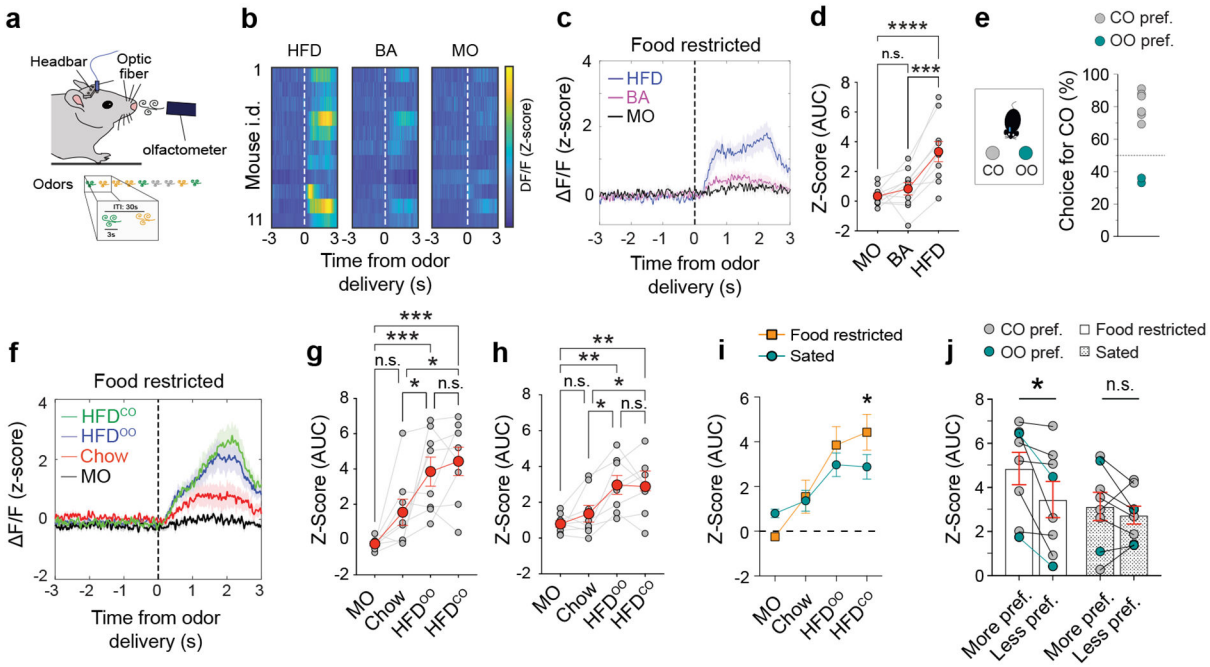

Figure 3. IPAC^{Nts} neurons encode the hedonic value of an odor

(a) A schematic of the experimental setup to test odor preference. **(b)** Heatmaps of average GCaMP6f responses of IPAC^{Nts} neurons in individual mice. Dashed line: stimulus presentation. HFD: high fat diet; BA: butyric acid; MO: mineral oil. **(c)** Average GCaMP6f signals from IPAC^{Nts} neurons in food-restricted mice to HFD, BA and MO. Dashed line: stimulus presentation. **(d)** Area under the curve (AUC) of the responses in individual mice measured in a 3-s window following the odor presentation. n=10 mice, $F_{(2,18)}$=21.06, p<0.0001; ***p<0.001, ****p<0.0001; One-way RM ANOVA, Holm-Sidak's test. **(e)** Mouse behavioral preference for coconut oil-based (HFD^{CO}) and olive oil-based (HFD^{OO}) high fat diets. **(f)** Average GCaMP6f signals from IPAC^{Nts} neurons of mice in (e), in food restriction, aligned to odor presentation (dashed line). **(g)** AUC of the responses of mice in (e, f), in food restriction, in a 3-s window following the odor presentation. Dashed line: stimulus presentation. N=8 mice, $F_{(3,21)}$=11.96, p<0.0001; n.s., p>0.05, *p<0.05, ***p<0.001; one-way RM ANOVA , Holm-Sidak's test. **(h)** AUC of the responses of mice in (e), sated, in a 3-s window following the odor presentation. N=8 mice, $F_{(3,21)}$=8.546, p= 0.0007; n.s., p>0.05, *p<0.05, **p<0.01; one-way RM ANOVA, Holm-Sidak's multiple comparisons test.

(i) Average responses of IPAC^{Nts} neurons in (g) and (h) are replotted for visual inspection. Interaction effect: $F_{(3,21)}$=5.394, p=0.0065; *p<0.05, two-way RM ANOVA, Holm-Sidak's test. **(j)** IPAC^{Nts} neurons responded more to the preferred than the non-preferred HFD in food-restricted mice (left), but not sated mice (right). N=8 mice.$F_{(1,7)}$=8.769, p=0.0211; p>0.05 (n.s), *p<0.05; two-way RM ANOVA, Holm-Sidak's test.

Data are presented as mean ± s.e.m.

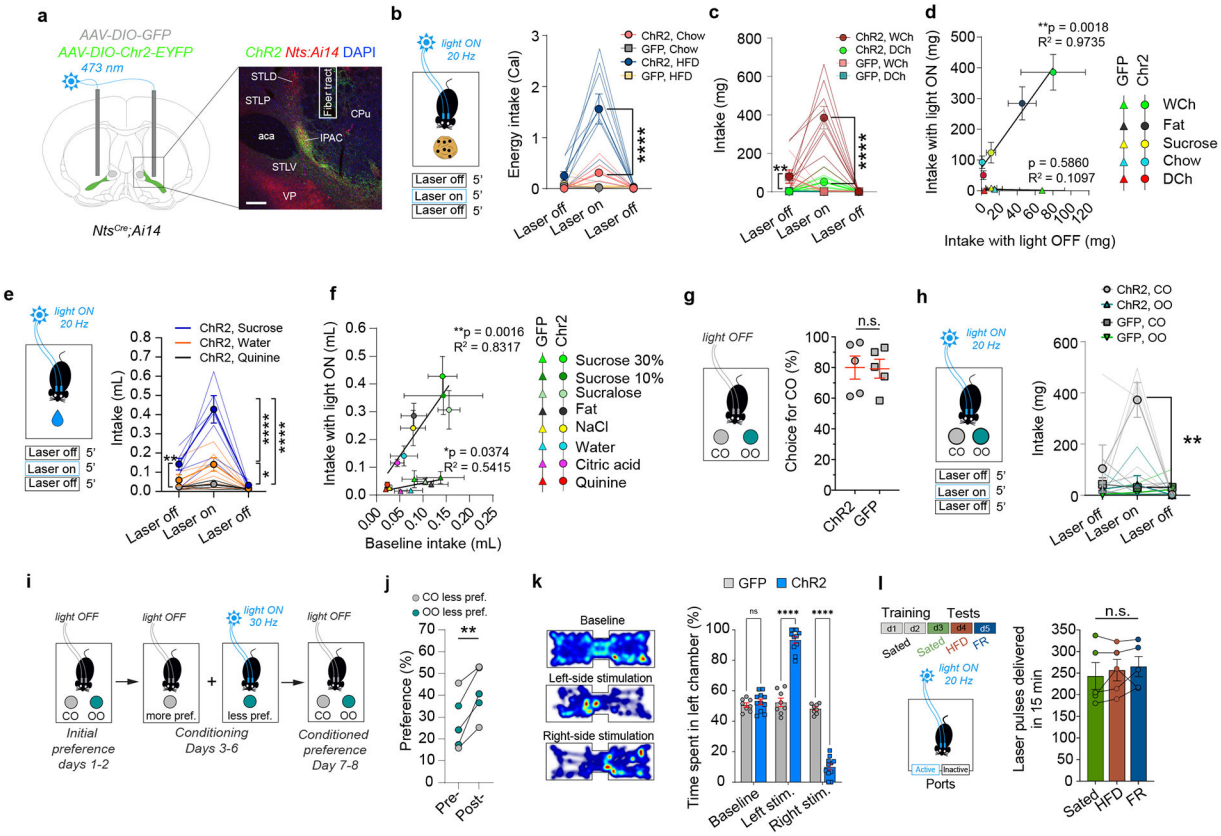

Figure 4. Activation of IPAC^{Nts} regulates dietary choices

(a) Representative histological image. Scale bar 200 μm. STLV/P/D: ventral/posterior/dorsal lateral division of the BNST; VP: ventral pallidum; CPu: caudate putamen; IPAC: interstitial nucleus of the posterior limb of the anterior commissure (aca). **(b)** Left: schematic of the paradigm. Right: intake of fed chow or HFD. ChR2 (n=9), interaction effect: $F_{(2,16)}$=17.75, p<0.0001, ****p<0.0001; GFP (n=8), group effect: $F_{(1,7)}$ = 9.164, p=0.0192, p>0.05(n.s.); two-way RM ANOVA, Sidak's test. **(c)** Intake of mice fed white or dark chocolate. ChR2 (n=9), $F_{(2,16)}$=19.12, p<0.0001, ****p<0.0001; GFP (n=6), $F_{(2,10)}$ = 5.6, p=0.0234, **p<0.001; two-way RM ANOVA, Sidak's test. **(d)** Correlation between food intake at baseline and during photostimulation. ChR2 (n=9): **p=0.0018; GFP (chow, sucrose, HFD, WhC: n=8; DCh: n=6), p = 0.5860 (n.s.); Pearson's test. **(e)** Liquid intake of ChR2 mice (n=7). interaction effect: $F_{(4,24)}$=14.90, p<0.0001, *p<0.05; ****p<0.0001; **p<0.001 between sucrose and quinine during the first laser off period; two-way RM ANOVA, Turkey's test. **(f)** Correlation between liquid intake at baseline and during photostimulation. ChR2 (n=7): **p=0.0016; GFP (n=5), *p=0.0374. Pearson's test. **(g)** Preference for HFD^{CO} over HFD^{OO} with light off. N=5 mice per group, p=0.9385 (n.s.), unpaired t-test. **(h)** Intake of mice (in g) on HFD^{CO} and HFD^{OO} with light on. ChR2 (n=5), interaction effect: $F_{(2,8)}$=9.443, p=0.0078, **p<0.01; GFP (n=5), interaction: $F_{(2,8)}$=0.9049, p=0.4423; two-way RM ANOVA, Sidak's test. **(i)** Paradigm for conditional flavor preference. **(j)** Effects of light delivery on food preference. N=5 mice per group, **p=0.0082, paired t-test. **(k)** Left: Heatmaps of a representative mouse in the RTPP/A task; Right: Preference of ChR2 (n=11) and GFP (n=8) mice for left chamber. Interaction effect: $F_{(2,34)}$=208.5; p<0.0001;

****p<0.0001; p>0.05 (n.s.), two-way RM ANOVA, Sidak's test. **(l)** Self-stimulation behavior of ChR2 mice (n=5) under different homeostatic states. $F_{(2,8)}$=1.463, p=0.2875 (n.s.), one-way ANOVA. Data are presented as mean ± s.e.m.

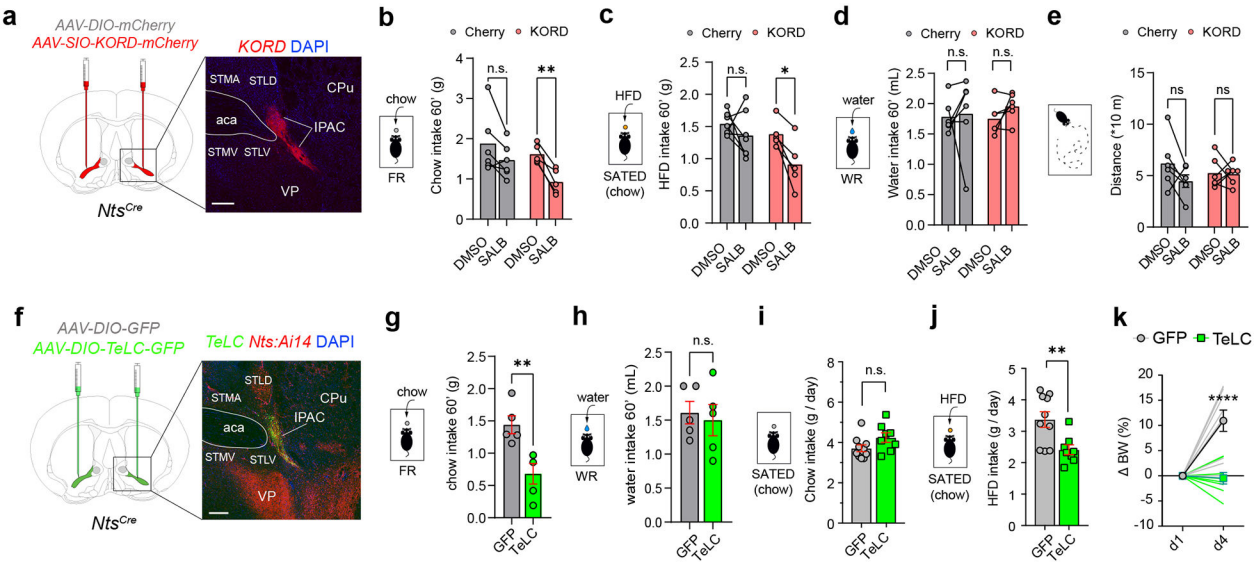

Figure 5. Inhibition and inactivation of IPAC^{Nts} neurons both disrupt feeding

(a) An image showing KORD expression in IPAC^{Nts} neurons in a representative *Nts^{Cre}* mouse. STLV/D: ventral/dorsal lateral division of the BNST; STMA/V: anterior medial/ventral division; VP: ventral pallidum; CPu: caudate putamen; IPAC: interstitial nucleus of the posterior limb of the anterior commissure (aca). Scale bar 200 μm. **(b)** Chow intake over a 1-h period in food-restricted (FR) *Nts^{Cre}* mice. mCherry mice, n=6; KORD mice, n=5. paired t-test. Cherry DMSO-SaLB: p=0.0785, (n.s.); KORD DMSO-SaLB: **p=0.0031. Paired t-test. **(c)** HFD intake over a 1-h period in sated *Nts^{Cre}* mice. mCherry mice, n=7; KORD mice, n=5. paired t-test. Cherry DMSO-SaLB: p=0.3194, (n.s.); KORD DMSO-SaLB: *p=0.0141. Paired t-test. **(d)** Water intake over a 1-h period in water restricted (WR) *Nts^{Cre}* mice. mCherry mice, n=6; KORD mice, n=6. paired t-test. Cherry DMSO-SaLB: p = 0.8725 (n.s.); KORD DMSO-SaLB: p=0.1672 (n.s.). Paired t-test. **(e)** Locomotion activity over a 1-h period in sated *Nts^{Cre}* mice. mCherry mice, n=6; KORD mice, n=6. paired t-test. Cherry DMSO-SaLB: p=0.1433 (n.s.); KORD DMSO-SaLB: p=0.8981 (n.s.). Paired t-test. **(f)** An image showing TeLC expression in IPAC^{Nts} neurons in a representative *Nts^{Cre}* mouse. Scale bar 200 μm. **(g)** Chow intake over a 1-h period in food-restricted (FR) *Nts^{Cre}* mice. GFP mice, n= 5; TeLC mice, n=5; **p=0.0071. Unpaired t-test. **(h)** Water intake over a 1-h period in water-restricted (WR) *Nts^{Cre}* mice. GFP mice, n=5; TeLC mice, n=5; p=0.7085 (n.s.). Unpaired t-test. **(i)** Daily chow intake over a 72-h period of *Nts^{Cre}* mice. GFP mice, n=10; TeLC mice, n=8; p=0.0785 (n.s.). Unpaired t-test. **(j)** Daily HFD intake over a 96-h period of *Nts^{Cre}* mice. GFP mice, n=10; TeLC mice, n=8; **p=0.0073. Unpaired t-test. **(k)** Acute changes in bodyweight (BW) following 4 days of HFD. Interaction effect: $F_{(1,16)}$=19.45, p=0.0004, ****p<0.0001. Two-way RM ANOVA followed by Sidak's multiple comparisons test. Data are presented as mean ± s.e.m.

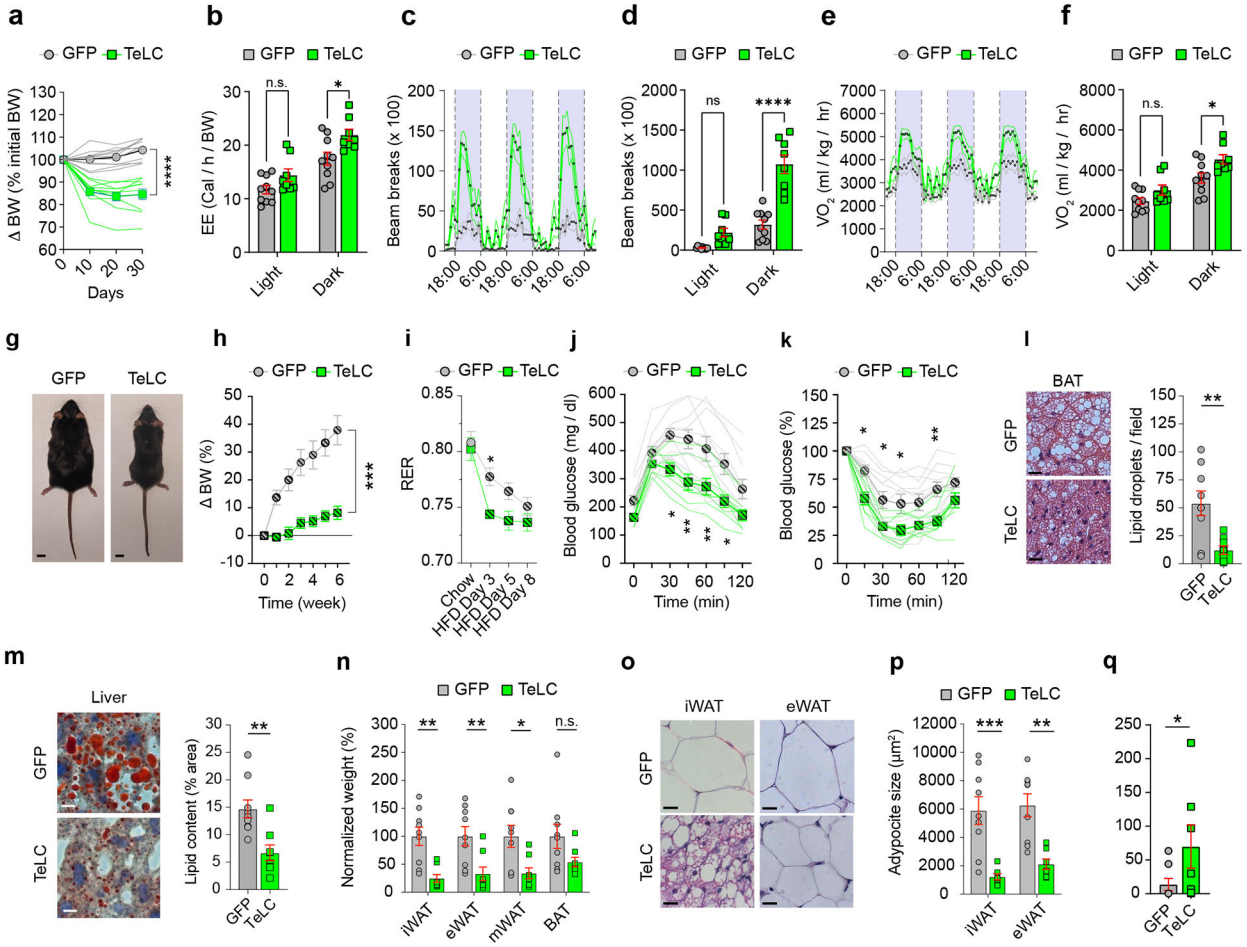

Figure 6. Inactivation of IPAC^{Nts} neurons protects from obesity and ameliorates metabolic syndrome

(a) Body weight (BW) of GFP (n=11) and TeLC mice (n=10) fed chow. Group effect: $F_{(1,19)}$=57.80, ****p<0.0001; two-way RM ANOVA, Sidak's test. **(b)** Energy expenditure of GFP (n=10) and TeLC mice (n=8) fed chow. Group effect: $F_{(1, 16)}$=5.934, p=0.0269; *p<0.05, p>0.05(n.s.); two-way RM ANOVA, Sidak's test. **(c, d)** Locomotor activity of GFP (n=10) and TeLC mice (n=8) fed chow. (c): Interaction effect: $F_{(70,1120)}$=7.699, p<0.0001, two-way RM ANOVA; (d): Group effect: $F_{(1,16)}$=37.84, p<0.0001; ****p<0.0001, p>0.05 (n.s.), two-way RM ANOVA, Sidak's test. **(e, f)** Oxygen consumed (VO_2) by GFP (n=10) and TeLC mice (n=8) fed chow. (e): Interaction effect: $F_{(70,1120)}$=2.221, p<0.0001, two-way RM ANOVA; (f): Group effect: $F_{(1, 16)}$=5.604, *p=0.0309, p>0.05 (n.s.); two-way RM ANOVA, Sidak's test. **(g)** A representative GFP and a TELC mouse under DIO. Scale bar: 1 cm. **(h)** Bodyweight (BW) of mice under DIO. GFP (n=10), TeLC (n=8). Group effect: $F_{(1, 16)}$=19.72, ***p<0.0004; two-way RM ANOVA. **(i)** RER of mice under DIO. GFP (n=10), TeLC (n=8). Group effect: $F_{(1, 16)}$=10.71, p=0.0048; *p<0.05; two-way RM ANOVA Sidak's test. **(j, k)** Blood glucose levels during GTT (j) and ITT (k) of mice under DIO. GFP (n=10), TeLC (n=8). (j): Group effect: $F_{(1, 16)}$=8.366, p=0.0106; (k): Group effect: $F_{(1, 16)}$=9.683, p=0.0067; *p<0.05, **p<0.01; two-way RM ANOVA, Sidak's test. **(l)** Left: BAT tissue of mice under DIO (H&E staining). Scale bar: 20 μm. Right: number of lipid

droplets in BAT. GFP (n=9); TeLC (n=8); **p=0.0037, unpaired t-test. **(m)** Left: liver tissue of mice under DIO (Red-Oil staining). Scale bar: 10 μm. Right: area of lipid droplets in liver. GFP (n=9); TeLC (n=8); **p=0.0025, unpaired t-test. **(n)** WAT weight, normalized to GFP mice. GFP (n=9); TeLC (n=8); group effect: $F_{(1,15)} = 9.757$, p=0.0070; *p<0.05, **p<0.01, p>0.05 (n.s.); two-way RM ANOVA, Sidak's test. **(o)** WAT of mice under DIO (H&E staining) . Scale bar: 20 μm. **(p)** Adipocyte size. Group effect: GFP (n=9); TeLC (n=7); $F_{(1,14)}$=19.8, p=0.0005; **p<0.01, ***p<0.001; two-way RM ANOVA followed by Sidak's multiple comparisons test. **(q)** Expression of *Ucp1* in iWAT of mice under DIO. GFP (n=8); TeLC (n=7); *p=0.0289, Mann Whitney U-test. Data are presented as mean ± s.e.m.

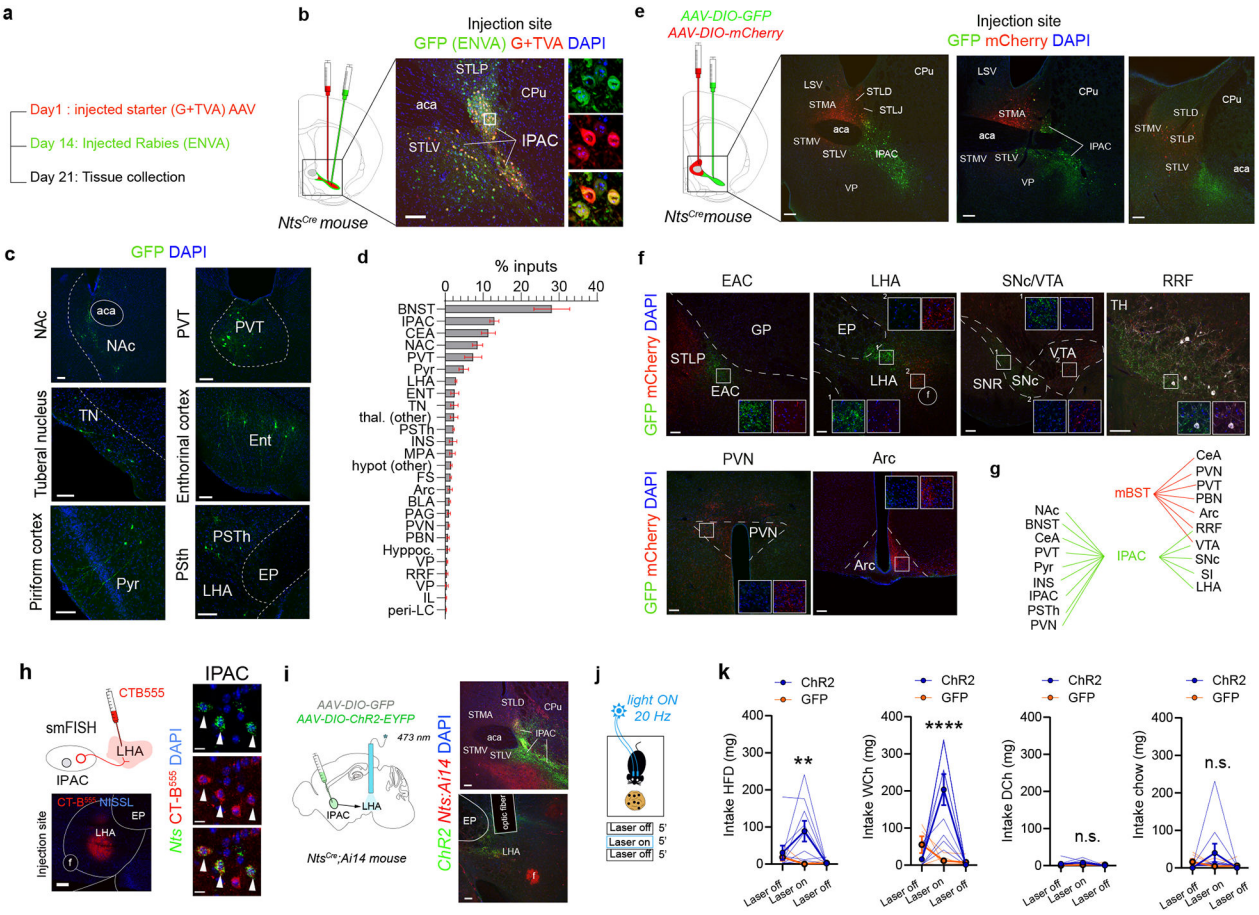

Figure 7. IPAC^{Nts} neurons send output and receive input to and from brain regions involved in energy homeostasis

(a) Schematic of the strategy for monosynaptic retrograde rabies virus tracing. **(b)** Representative image of the injection site. STLV/P/D/J: ventral/posterior/dorsal/juxtacap lateral division of the BNST; STMA/V: anterior medial/ventral division; VP: ventral pallidum; CPu: caudate putamen; IPAC: interstitial nucleus of the posterior limb of the anterior commissure (aca); LHA: lateral hypothalamus; EP: endopeduncular nu. NAc: Nucleus accumbens; Hyp: hypothalmus, GP: globus pallidus EAC: sublent. Ext. amygdala cent., SNR: substantia nigra, reticular; SNC: substantia nigra, compact; VTA: ventral tegmental area RRF: retrorubral field; PVN: paraventricular nu.; Arc: arcuate hyp. nu; PVT: paraventricular thalamic nu.; PSTh: Prasubthalamic nu. Scale bar: 100 μm. **(c)** Representative images of the areas projecting to IPAC^{Nts} neurons. Scale bar: 100 μm. **(d)** Brain regions projecting to IPAC^{Nts} neurons (n=3). **(e)** Representative images of the injection sites from a *Nts^{Cre}* mouse injected with multi-color *Cre*-dependent AAVs (GFP in IPAC; mCherry in mBNST). Scale bar: 200 μm. **(f)** Representative images of brain areas innervated by IPAC^{Nts} (green) and mBNST^{Nts} (red) neurons. Scale bar: 100 μm. **(g)** Diagram illustrating brain region upstream and downstream of IPAC^{Nts} neurons. **(h)** Schematic of the retrograde strategy to label IPAC^{Nts} neurons projecting to the LHA (left, top panel), representative image of the injection site (left, bottom panel, scale bar: 200μm) and of FISH for *Nts* on retrograde labelled CT-B^{+} neurons in the IPAC (right, scale bar:

10μm). **(i)** Left: schematic of the strategy to activate the $IPAC^{Nts}$ → LHA pathway; Right: representative image showing ChR2 expression in $IPAC^{Nts}$ neurons and an optical-fiber tract on the LHA from a representative *Nts^{Cre};Ai14* mouse. Scale bar 100 μm. **(j)** Schematic of the paradigm for testing the effects of optogenetics on feeding behavior. **(k)** Effect of light delivery into the LHA of mice injected in the IPAC with ChR2 or GFP mice and fed HFD, WCh, DCh, chow. ChR2 mice (n=9), GFP mice (n=5). HFD, interaction effect: $F_{(2,24)}$=3.834, p=0.0359; WCh, interaction: $F_{(2,24)}$=13.19, p=0.0001; DCh, interaction effect: $F_{(2,24)}$=1.807, p=0.1858; Chow, interaction effect: $F_{(2,24)}$=1.756, p=0.1942. Two-way RM ANOVA, Sidak's test. **p<0.01, ****p<0.0001, p>0.05 (n.s.).